Reactor noise measurements in the UTR-10 using the polarity correlation method

by

Massoud Nabavian

A Thesis Submitted to the
Graduate Faculty in Partial Fulfillment of
The Requirements for the Degree of
MASTER OF SCIENCE

Major: Nuclear Engineering

Iowa State University
Ames, Iowa

1973

TABLE OF CONTENTS

		Page
I.	INTRODUCTION	1
II.	LITERATURE SURVEY	2
III.	THEORY OF THE COHERENCE FUNCTION FORMULATION	6
	A. Background	6
	B. Reactor Noise Source	7
	C. Reactor Transfer Function	10
	D. Pile Noise Effect on Detectors	12
	E. Auto-spectral Density	14
	F. Cross-spectral Density	19
	G. Coherence Function	20
IV.	SHUTDOWN REACTIVITY FROM THE COHERENCE FUNCTION	27
	A. Case of Identical Detectors	27
	B. Case of Non-Identical Detectors	27
	C. Detection Efficiency Dependence of Subcriticality Measurements	28
V.	MEASUREMENT OF THE COHERENCE FUNCTION	33
	A. Polarity Correlation Method	33
	B. Dynamic Filtering	36
	C. Errors and Uncertainties	37
VI.	EQUIPMENT AND PROCEDURES	41
VII.	DISCUSSION AND RESULTS	48
	A. Coherence Function Measurements	48

		Page
	B. Subcritical Reactivity Measurements	57
VIII.	SUMMARY AND CONCLUSIONS	61
IX.	SUGGESTIONS FOR FURTHER WORK	63
X.	LITERATURE CITED	64
XI.	ACKNOWLEDGMENTS	67
XII.	APPENDIX A: REACTOR NOISE SOURCE FORMULATION	68
XIII.	APPENDIX B: REACTOR OPEN LOOP TRANSFER FUNCTIONS FORMULATION	71
	A. Source Transfer Function	72
	B. Reactivity Transfer Function	75
XIV.	APPENDIX C: CROSS SPECTRAL DENSITY FORMULATION	78
XV.	APPENDIX D: SUBCRITICAL REACTIVITY FORMULATIONS	83
XVI.	APPENDIX E: THEORETICAL COHERENCE FUNCTION FORMULATION	88
XVII.	APPENDIX F: RESULTS OF COHERENCE FUNCTION MEASUREMENT AT 4.5" FROM THE SOUTH TANK	91

I. INTRODUCTION

The method of noise analysis as a useful tool in the investigation of the kinetic behavior of nuclear systems has become very widespread. The methods used to extract information from reactor noise are quite varied. In early work only one detection channel was used to gather information. With the advent of two detection channel systems it became possible to reduce the effect of extraneous noise in the system by cross correlating the outputs of the two detection channels. The method of coherence function measurement additionally eliminates (theoretically) the effect of signal analysis system frequently response on the signal being studied.

It has been shown that the polarities of the two signals in a two channel noise analysis system carry enough information to allow reactor noise signals to be analyzed by the method of polarity cross-correlation. Thus, the coherence function measurement offers a good method of measuring prompt neutron decay constant as well as subcritical reactivity in a nuclear reactor.

The objective of this study is to explore the theory, and to make experimental measurements of the coherence function, prompt neutron decay constant, and shutdown reactivities for the UTR-10 reactor, using the method of polarity cross-correlation.

II. LITERATURE SURVEY

This section contains a brief survey of contributions to the field of reactor noise analysis in general, leading to the advent of the polarity correlation method for noise analysis, coherence function measurements, and subcritical reactivity measurements. A survey of papers suggesting improvements in the coherence function measurements and subcriticality measurements by the method of polarity correlation is then given.

Many options and combination of options are available to the designer of a reactor noise analysis system. One option is the choice of input signal. Experiments by Balcomb [3], Stern [32], and Valat [34] used externally applied signals. Other experiments such as those of Cohn [10], Danofsky [13], and Seifritz et al. [30], relied on the natural stochastic processes of fission, capture, etc., for the random noise input signal with no externally applied input.

The second option in noise analysis method is the choice of analyzing the signal in the frequency or the time domain. Balcomb et al. [4], Dragt [15], and Rajagopal [25] performed experiments in the time domain, while Badgley and Uhrig [2] and Seifritz [29] conducted investigations in the frequency domain.

The third option of the experimenter in reactor noise analysis is the number of detection channels to be used. Early experiments by Balcomb et al. [4], Cohn [10], and

Rajagopal [25] used only one detection channel to determine the output signal. Use of only one detection channel requires that detector efficiency be high enough to make the reactor noise signal observable above the random detection noise. The efficiency requirements can be relaxed somewhat by the use of two detection channels. Cross correlation of the signals from these two channels enhances the signal and rejects the uncorrelated noise. This type of cross correlation was used in investigations by Kryter et al. [22], and Hendrickson [19].

Recently the use of the polarity correlation technique in reactor noise analysis has received much attention. In the polarity correlation process only the signs of the signals, with respect to their mean values, are correlated. Theoretical investigations by Pacilio [24], and experimental investigations by Dragt [14] and Seifritz [29] have demonstrated that the polarity of the signals contains sufficient information to allow reactor noise to be analyzed by this method.

Cohn [11] proposed a noise-equivalent source obtained from the Schottky formula which calculates the noise due to the random flow of electrons in a diode. The analogy to production, absorption, and leakage of neutrons holds because all of these processes obey the Poisson distribution. It was noted that the spectral density of the noise-equivalent source for prompt neutrons is independent of frequency, and thus the noise input is white.

Seifritz [29] used a two-detector cross-correlation method of zero-power reactor noise analysis to determine characteristic kinetic reactor parameters. This method, called polarity correlation in the frequency domain, is based on the detailed analysis of the stochastic coherence function, in contrast to the analysis of auto and/or cross power spectral density functions. The coherence function was obtained by polarity correlation of two filtered random neutron noise signals simultaneously sampled in a reactor system using neutron sensitive detectors in the current mode of operation. The advantage of using this technique is both its simplicity and the automatic elimination of the equipment frequency response. Furthermore, shutdown reactivity measurements were made using the polarity correlation method.

Analysis of the precision of the coherence function measurements was done by Seifritz [29] and the results were also later reported by Vaurio [35]. Errors in the polarity correlation method of reactivity measurements were calculated by Hess and Albrecht [20] using Korn and Korn [21] equation for the variance of the coherence function.

Effect of gamma radiation on subcriticality measurements using noise analysis were considered by Roux and Buhl [27]. They showed that residual gamma radiation reduces the signal-to-noise ratio and hence the precision of a subcriticality measurement. They proposed that ^{235}U fission chambers are the

best choice compared to ^{10}B and ^{3}He detectors in high gamma fields.

Ackermann and Buhl [1] suggested that a systematic error in the subcritical reactivity measurement may occur due to unexpected changes in the neutron detection efficiencies of the detectors. They proceeded by developing new equations for subcriticality by taking into account the changes that might occur in detector efficiencies.

Yasuda and Miyoshi [36] applied the polarity correlation method of noise analysis to a graphite moderated reactor. They suggested that in graphite and heavy-water moderated reactors with long prompt neutron lifetime, it is difficult to measure the prompt neutron decay constant, especially at near critical state. The reasons for this are, very low signal to noise ratio, because of many independently occurring prompt neutron decay chains, which overlap each other, and that the mean lifetime of the precursors to the short-lived delayed neutrons is not sufficiently longer than the lifetime of the prompt neutrons. This complicates the separation of the prompt neutron decay mode from the associated delayed neutron mode.

III. THEORY OF THE COHERENCE FUNCTION FORMULATION

A. Background

In the following sections it is shown how the coherence function can be derived using the reactor noise source, reactor transfer function, auto-spectral densities, and cross-spectral densities.

It will be shown that the coherence function is related to the prompt neutron decay constant, α_c. The prompt neutron decay constant is defined as

$$\alpha_c = \beta/\ell = \beta v \Sigma_a \ , \tag{1}$$

where β is the delayed neutron fraction,

ℓ is the prompt neutron lifetime,

Σ_a is the total macroscopic absorption cross section for the thermal neutrons, and

v is the thermal neutron velocity.

Basic information about impulse response, convolution, transfer functions, correlation functions, and Fourier transforms of correlation functions, viz, the spectral density functions, can be found in texts by Bendat [5], Bendat and Piersol [6], Brown and Nilsson [8], and Uhrig [33].

B. Reactor Noise Source

In most reactor physics work the neutrons are treated as a continuous fluid instead of discrete particles. For most purposes, this is quite adequate. However, the discreteness of the neutrons and the statistical nature of the chain reaction give rise to random fluctuations in reactor power level which may be characterized by the term "pile noise".

The pile noise may be considered as arising from a random "noise equivalent" neutron source driving the reactor, which represents the fluctuations in the number of neutrons available to the reactor caused by the natural statistical fluctuations in the rates of neutron absorption and fission. At any instant this source may be either positive or negative, representing, respectively, an excess or a deficiency from the average.

The production, absorption, and leakage of neutrons in a reactor may be considered analogous to the random flow of electrons in a diode, because all of these processes obey the Poisson distribution. Therefore, the magnitude of the noise - equivalent source may be obtained from the Schottky formula, which was originally developed to calculate the noise in a temperature-limited electronic diode. It is usually written in the form

$$\langle |I|^2 \rangle = 2e^2\bar{m} \ , \qquad (2)$$

where $\langle |I|^2 \rangle$ is the spectral density of the diode current noise in amps^2 sec^{-1}, e is the charge carried by each electron in coulombs, and $\bar{m}$ is the average number of electrons flowing per second.

For calculating the noise-equivalent neutron source the above formula is modified in form by Cohn [11], and is written as

$$\Phi_{ns} = 2 \sum_i q_i^2 \bar{m}_i \ . \qquad (3)$$

Here Φ_{ns} is the spectral density of the noise equivalent source in neutrons^2 sec^{-1}, q_i is the net number of neutrons produced in the occurrence of one nuclear reaction of type i, and $\bar{m}_i$ is the average number of reactions of type i occurring per second in the reactor. The summation is taken over all possible types of nuclear reactions which may occur in the reactor.

The term "spectral density" used above is defined as the mean square amplitude of that part of the noise contained in a given narrow frequency band, divided by the band width in cycles per second.

It is shown in Appendix A that the spectral density of the noise equivalent neutron source is given by

$$\Phi_{ns} = \frac{2n\bar{\nu}D}{\ell} \ , \qquad (4)$$

where n is the neutron density in the reactor, $\bar{\nu}$ is the average number of neutrons released per fission and D is the Diven factor defined as $D = \overline{(\nu^2 - \bar{\nu})}/\bar{\nu}^2$.

The spectral density of the equivalent reactivity fluctuations, Φ_{nn}, may be obtained from the expression

$$\Phi_{nn} = (\frac{\ell}{n})^2 \Phi_{ns} \quad , \tag{5}$$

because a small reactivity fluctuation ρ can be looked upon as supplying to a critical reactor a source of strength $\rho n/\ell$ neutrons per second so long as the resulting fluctuations in n remain small. Inserting Equation 4 in 5, we get

$$\Phi_{nn} = \frac{2\ell\bar{\nu}D}{n} \quad . \tag{6}$$

It is obvious from the Equations 4 and 6 that the spectral density of the noise-equivalent source and hence the spectral density of the equivalent reactivity fluctuations are independent of frequency, and thus represent white noise. According to Cohn [11] this will hold true up to frequencies of the order of the reciprocal of the time required for the complete transition between the bound and unbound quantum states of the neutron, which is less than 10^{-20} seconds.

In deriving Equation 6 the effect of delayed neutrons was ignored, and it was assumed that there were no extraneous neutron sources in the reactor. This model is sufficient for the present work. Sheff and Albrecht [31] have developed a

neutron noise source model which includes the effect of delayed neutrons, extraneous sources, non-whiteness of fission neutron spectrum, and separate accounting of absorption processes in the reactor.

C. Reactor Transfer Function

In this section, two types of open loop transfer functions for a reactor are given. These are the so called source and reactivity transfer functions.

The transfer function of a system is defined as the ratio of the Laplace transforms of the output to the input with zero initial conditions. In the present case the output is considered to be a small variation in the neutron level and the input is a small varying source or a small varying reactivity for the source and reactivity transfer functions respectively. That is

$$H_s(s) = \frac{L(\text{output neutron variation})}{L(\text{input source variation})} = \frac{\Delta N(s)}{\Delta S(s)} \tag{7}$$

$$H_r(s) = \frac{L(\text{output neutron variation})}{L(\text{input reactivity variation})} = \frac{\Delta N(s)}{\Delta R(s)} \tag{8}$$

where $H_s(s)$ is the source transfer function and $H_r(s)$ is the reactivity transfer function.

The open loop or zero power transfer function of a nuclear reactor is the transfer function of the reactor based only on delayed neutron effects and neglecting all feedback

effects. This type of transfer function is theoretically formulated from space independent reactor kinetic equations, or a point reactor model.

The formulation of source and reactivity transfer functions for the case of a single delayed neutron group are given in Appendix B. The square modulus of the source transfer function for one delayed neutron group and a subcritical reactor is

$$|H_s(\omega)|^2 = \frac{1}{\alpha_c^2} \frac{1}{(1-\$)^2 + (\omega/\alpha_c)^2} , \qquad (9)$$

which reduces to

$$|H_s(\omega)|^2 = \frac{1}{\alpha_c^2} \frac{1}{1 + (\omega/\alpha_c)^2} , \qquad (10)$$

for a critical reactor.

The square modulus of the reactivity transfer function for one delayed neutron group and subcritical reactor is

$$|H_r(\omega)|^2 = \left(\frac{n_o}{\beta}\right)^2 \frac{1}{(1-\$)^2 + (\omega/\alpha_c)^2} , \qquad (11)$$

which reduces to

$$|H_r(\omega)|^2 = \left(\frac{n_o}{\beta}\right)^2 \frac{1}{1 + (\omega/\alpha_c)^2} , \qquad (12)$$

for a critical reactor.

In the above equations ω is frequency in radians per second, α_c is the prompt neutron decay constant defined as $\alpha_c = \beta/\Lambda$ where β is the one-group delayed neutron fraction, $\Lambda = \ell/k$ is neutron generation time, n_o is neutron density at steady state, and \$ represents the subcriticality of the reactor in dollars.

In the above equations for square moduli of transfer functions it is assumed that $\omega >> \bar{\lambda}$, where $\bar{\lambda}$ is the average delayed neutron precursor decay constant. If this simplifying assumption is not used and all 6 delayed groups are considered the critical reactor reactivity transfer function will become

$$H_r(s) = \frac{\Delta N(s)}{\Delta R(s)} = \frac{n_o}{\ell} \frac{1}{s\left[1 + \sum_{i=1}^{6} \frac{\beta_i}{\ell(s+\lambda_i)}\right]}, \qquad (13)$$

where β_i are the individual delayed neutron fractions and λ_i are the individual delayed neutron precursor decay constants. The derivation of Equation 13 is given by Schultz [28].

D. Pile Noise Effect on Detectors

Since the pile noise must be observed in order to be useful, the process of observation must be considered. This observation is commonly done by means of a detector such as an ionization chamber which absorbs some of the neutrons in the reactor and produces an electrical signal. Consider that this detector collects a fraction ε of all the neutrons

absorbed in the reactor in whatever manner. The average current $\bar{I}$ passing through the chamber will then be given by

$$\bar{I} = \frac{\varepsilon \bar{q} n}{\ell} , \tag{14}$$

where $\bar{q}$ is the average charge transferred per neutron absorbed, and n is total number of neutrons in the reactor. Superimposed on this current will be fluctuating currents which arise in two ways. First, fluctuations will be produced by the pile noise fluctuations in the reactor neutron population to which the chamber is exposed. The spectral density of these fluctuations is given by Cohn [11] as

$$\frac{W^2 \bar{q}^2}{\bar{\nu}^2 \ell^2} \left| H_r(\omega) \right|^2 \Phi_{nn}(\omega) , \tag{15}$$

where $$W = \bar{\nu}\varepsilon \tag{16}$$

is the detector efficiency defined as neutrons detected per fission in the reactor, and $\Phi_{nn}(\omega)$ is the source spectral density defined by Equation 6.

Secondly, since the steady current $\bar{I}$ in the chamber is made up of many pulses of current produced by randomly arriving neutrons, there will be a white noise component due to the statistical nature of this detection process. Its spectral density can be obtained from Equation 2 and is given by Cohn [11] as

$$\Phi_d(\omega) = \frac{2\bar{q}^2 Wn}{\ell\bar{\nu}} . \tag{17}$$

Since these two noise components are to first order uncorrelated if $\varepsilon << 1$, their spectral densities add in quadrature, giving for the total current noise in the chamber output

$$\Phi_q(\omega) = \frac{2\bar{q}^2 Wn}{\ell\bar{\nu}} + \frac{W^2\bar{q}^2}{\bar{\nu}^2\ell^2} |H_r(\omega)|^2 \Phi_{nn}(\omega). \tag{18}$$

Thus the relative proportion of pile noise to white noise in the chamber output signal depends on the detection efficiency W.

E. Auto-spectral Density

The signal flow diagram resulting in two signals x(t) and y(t), the outputs of two independent and non-identical detection channels, is shown in Figure 1. The auto-correlation function of a zero mean signal b(t) is by definition

$$\phi_{bb}(\tau) = \lim_{T\to\infty} \frac{1}{2T} \int_{-T}^{T} b(t)b(t+\tau)dt. \tag{19}$$

The auto-spectral density of b(t) is the Fourier transform of $\phi_{bb}(\tau)$ or

$$\Phi_{bb}(\omega) = \int_{-\infty}^{\infty} \phi_{bb}(\tau)\, e^{-j\omega\tau}\, d\tau. \tag{20}$$

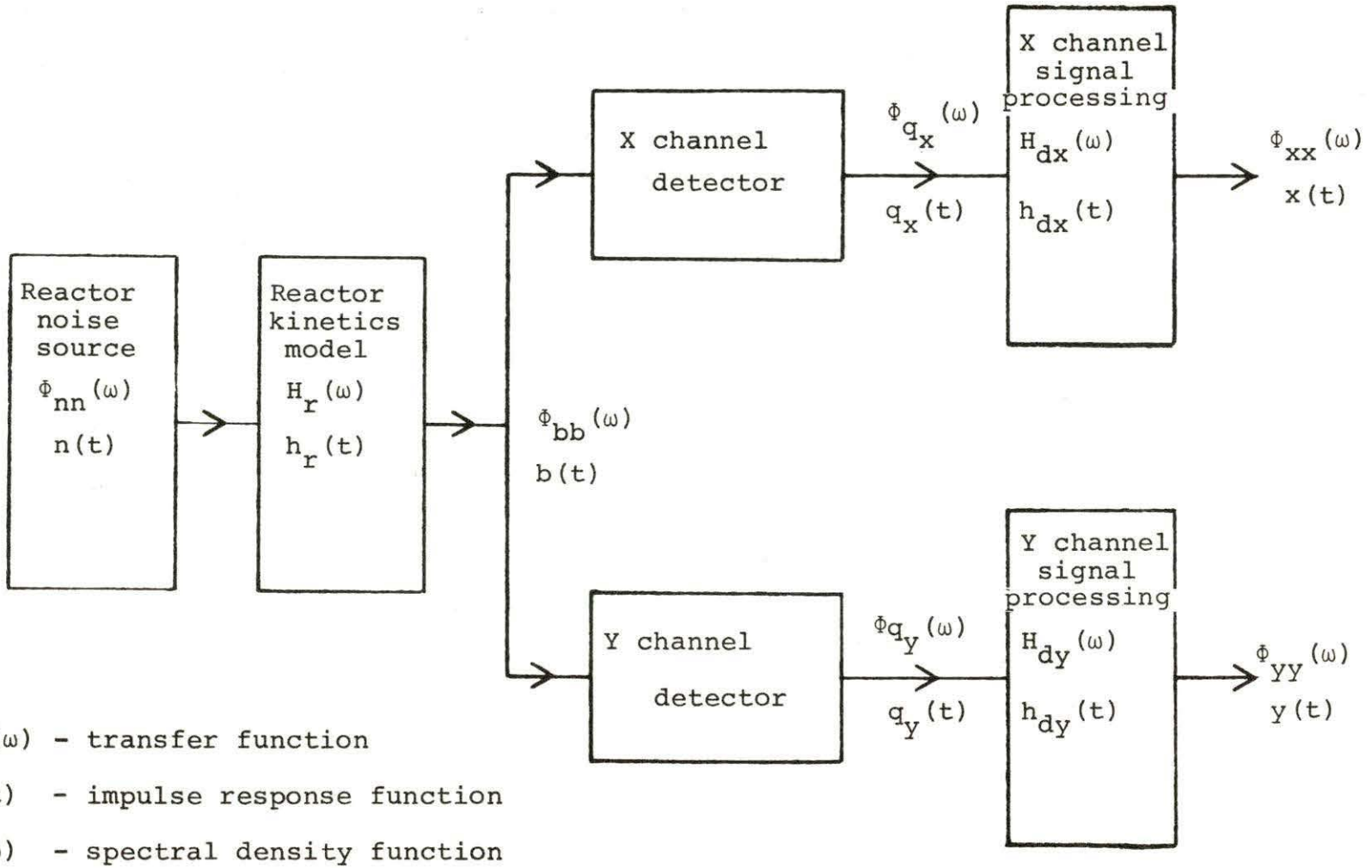

$H_r(\omega)$ - transfer function

$h(t)$ - impulse response function

$\Phi(\omega)$ - spectral density function

Figure 1. Signal flow diagram

It can be shown [33] that the auto-spectral density of a system is equal to the square modulus of the transfer functions of the system times the input auto-spectral density. Thus

$$\Phi_{bb}(\omega) = |H_r(\omega)|^2 \Phi_{nn}(\omega). \tag{21}$$

The spectral output of an ionization chamber was defined by Equation 18. For the two non-identical detectors considered here the spectral outputs can be written as

$$\Phi_{q_x}(\omega) = \frac{2\bar{q}^2 W_x n}{\ell \bar{\nu}} + \frac{W_x^2 \bar{q}^2}{\bar{\nu}^2 \ell^2} |H_r(\omega)|^2 \Phi_{nn}(\omega) , \tag{22}$$

and

$$\Phi_{q_y}(\omega) = \frac{2\bar{q}^2 W_y n}{\ell \bar{\nu}} + \frac{W_y^2 \bar{q}^2}{\bar{\nu}^2 \ell^2} |H_r(\omega)|^2 \Phi_{nn}(\omega) , \tag{23}$$

where Φ_{q_x} and Φ_{q_y} are the spectral outputs of the two detectors x and y and W_x and W_y are their efficiencies.

The concept introduced in Equation 21 leads to the auto-spectral densities of the output signals x(t) and y(t);

$$\Phi_{xx}(\omega) = |H_{dx}(\omega)|^2 \Phi_{q_x}(\omega) , \tag{24}$$

and

$$\Phi_{yy}(\omega) = |H_{dy}(\omega)|^2 \Phi_{q_y}(\omega) , \tag{25}$$

where $H_{dx}(\omega)$ and $H_{dy}(\omega)$ are the transfer functions of the two signal processing channels.

A reasonable simplifying assumption will be introduced at this point. It will be assumed that the two signal processing channels affect the amplitudes of the two signals x(t) and y(t) through unequal gain factors, only. With this in mind we can write

$$|H_{dx}(\omega)|^2 = A_x^2(\omega) \; |H_d(\omega)|^2 \; , \tag{26}$$

and

$$|H_{dy}(\omega)|^2 = A_y^2(\omega) \; |H_d(\omega)|^2 \; . \tag{27}$$

Substituting in Equations 24 and 25, we have

$$\Phi_{xx}(\omega) = A_x^2(\omega) \; |H_d(\omega)|^2 \; \Phi_{qx}(\omega) \; , \tag{28}$$

and

$$\Phi_{yy}(\omega) = A_y^2(\omega) \; |H_d(\omega)|^2 \; \Phi_{qy}(\omega) \; . \tag{29}$$

In Equations 22 and 23, the second term is the reactor noise contribution, while the first term is the detection noise contribution. A ratio of correlated reactor noise to uncorrelated detection noise, or a signal-to-noise ratio, can be defined as

$$Q_n(\omega) = \frac{\frac{W_n^2 \bar{q}^2}{\bar{\nu}^2 \ell^2} \; |H_r(\omega)|^2 \; \Phi_{nn}}{\Phi_{dn}(\omega)} \; , \tag{30}$$

where the subscripts n = x,y refer to either channel x or y except for Φ_{nn} and Φ_{ns}. Upon substitution of Equations 6, 11 and 17, Equation 30 reduces to

$$Q_n(\omega) = \frac{W_n D/\beta^2}{(1-\$)^2 + (\omega/\alpha_c)^2} = \frac{Q_{n,m,c}}{(1-\$)^2 + (\omega/\alpha_c)^2} , \quad (31)$$

where

$$Q_{n,m,c} = \frac{W_n D}{\beta^2} \quad (32)$$

is the maximum signal-to-noise ratio at delayed critical ($\$=0$) and low frequency ($\omega << \alpha_c$).

When the effects of the statistical nature of the detection chamber ionization process are included, as was done by Seifritz [29], the maximum ratio of reactor noise to detection noise is reported as

$$Q_{n,m,c} = \frac{W_n D}{R\beta^2} , \quad (33)$$

where R is the "Bennett factor" defined as

$$R = \frac{\overline{q^2}}{\bar{q}^2} . \quad (34)$$

In either case, the importance of detector efficiency in making the correlated reactor noise signal observable above the uncorrelated detection noise in the auto-spectral densities, $\Phi_{xx}(\omega)$ and $\Phi_{yy}(\omega)$, is apparent since the ratio is directly proportional to W_n, the detector efficiency.

In deriving Equation 33 for maximum signal-to-noise ratio, the effect of gamma radiation was ignored. Roux and Buhl [27] have shown that current induced in the detectors by gamma

radiation can reduce the signal-to-noise ratio significantly if the gamma field is intense ($>10^5$R/h) near the detectors. This kind of situation could arise if a reactor is operated at high power and then shut down. The signal-to-noise ratio is degraded by a factor $C = (U_n + U_\gamma)/U_n$, where U_n and U_γ are the uncorrelated noise due to neutrons and γ-rays respectively. The signal-to-noise ratio of Equation 33 will take the form

$$Q_{n,m,c} = \frac{W_n D}{R\beta^2 C} . \tag{35}$$

The effect of gamma radiation degradation of signal-to-noise ratio will be kept to a minimum in this work by controlling the experimental procedures. This could be easily achieved by not making measurements right after the reactor has been operated at high power.

F. Cross-spectral Density

It has been previously mentioned that the use of two detection systems enhances the rejection of the random detection system noise. This follows from the formulation of the cross-spectral density function given in Appendix C. The cross-spectral density of two signals x(t) and y(t) is shown to be

$$\Phi_{xy}(\omega) = W_x W_y A_x(\omega) A_y(\omega) |H_d(\omega)|^2 \Phi_{ii}(\omega) , \tag{36}$$

where $\Phi_{ii}(\omega)$ is the spectral density of a common signal in both detectors. From Equations 22 and 23 it is easily seen that

$$\Phi_{ii}(\omega) = \frac{\bar{q}^2}{\bar{\nu}^2 \ell^2} |H_r(\omega)|^2 \Phi_{nn}(\omega) . \tag{37}$$

After substituting this in Equation 35 the cross-spectral density function of x(t) and y(t) becomes

$$\Phi_{xy}(\omega) = W_x W_y A_x(\omega) A_y(\omega) \frac{\bar{q}^2}{\bar{\nu}^2 \ell^2} |H_d(\omega)|^2 |H_r(\omega)|^2 \Phi_{nn}(\omega) . \tag{38}$$

It is readily seen that this cross-spectral density function is independent of $\Phi_{dx}(\omega)$ and $\Phi_{dy}(\omega)$, which are the uncorrelated parts of the spectral outputs of the detectors, and arise from the random detection system noise.

G. Coherence Function

The inherent advantage in introducing the coherence function is that it is independent of the detection system transfer function, $H_d(\omega)$, appearing in the definitions of the auto- and cross-spectral densities given in Equations 28, 29 and 38.

This independence is achieved by the way that the coherence function is defined. The coherence function of two signals x(t) and y(t) is by definition [29]

$$\gamma(\omega) = \frac{\Phi_{xy}(\omega)}{[\Phi_{xx}(\omega)\ \Phi_{yy}(\omega)]^{1/2}} \cdot \tag{39}$$

This definition of coherence function is commonly used in the literature, but Bendat and Piersol [6] and Uhrig [33] have called $\gamma^2(\omega)$ the coherence function. In this work the definition given by Equation 39 will be used for the coherence function.

The spectral densities can be replaced in Equation 39 by Equation 28, 29 and 38. The result is

$$\gamma(\omega) = \frac{W_x W_y A_x(\omega) A_y(\omega)\ \frac{\bar{q}^2}{\bar{v}^2 \ell^2}\ |H_d(\omega)|^2 |H_r(\omega)|^2\ \Phi_{nn}(\omega)}{A_x(\omega) A_y(\omega) |H_d(\omega)|^2 [\Phi_{q_x}(\omega) \cdot \Phi_{q_y}(\omega)]^{1/2}}$$

$$= \frac{W_x W_y\ \frac{\bar{q}^2}{\bar{v}^2 \ell^2}\ |H_r(\omega)|^2\ \Phi_{nn}(\omega)}{[\Phi_{q_x}(\omega) \cdot\ \Phi_{q_y}(\omega)]^{1/2}} \cdot \tag{40}$$

It is now evident from Equation 40 that the coherence function is independent of $H_d(\omega)$. If $\Phi_{nn}(\omega)$, $|H_r(\omega)|^2$, $\Phi_{q_x}(\omega)$ and $\Phi_{q_y}(\omega)$ are replaced by Equations 6, 11, 22 and 23 respectively, and the definition given in Equation 31 is used, $\gamma(\omega)$ could be written as

$$\gamma(\omega) = \left[\frac{Q_x(\omega) \cdot Q_y(\omega)}{[1 + Q_x(\omega)][1 + Q_y(\omega)]} \right]^{1/2} \tag{41}$$

where $Q_x(\omega)$ and $Q_y(\omega)$ are defined by Equation 31 as

$$Q_n(\omega) = \frac{Q_{n,m,c}}{(1-\$)^2 + (\omega/\alpha_c)^2} , \tag{42}$$

where

$$Q_{n,m,c} = \frac{W_n D}{R\beta^2} , \tag{43}$$

and n = x,y depending on the channel specified.

If it is assumed that the detector efficiencies are equal ($W_x = W_y = W$), the coherence function takes the form

$$\gamma(\omega) = \frac{Q(\omega)}{1 + Q(\omega)} , \tag{44}$$

where

$$Q(\omega) = \frac{Q_{m,c}}{(1-\$)^2 + (\omega/\alpha_c)^2} , \tag{45}$$

and

$$Q_{m,c} = \frac{DW}{R\beta^2} , \tag{46}$$

or

$$\gamma(\omega,\$) = \frac{Q_{m,c}}{(1-\$)^2 + Q_{m,c} + (\omega/\alpha_c)^2} . \tag{47}$$

If it is further assumed that the reactor is critical ($=0), the coherence function becomes

$$\gamma_c(\omega) = \frac{Q_{m,c}}{1 + Q_{m,c} + (\omega/\alpha_c)^2} . \tag{48}$$

Examination of Equation 48 shows that the coherence function has a low frequency plateau value of

$$\gamma_{c,o} = \gamma_c(\omega << \alpha_c) = \frac{Q_{m,c}}{1 + Q_{m,c}} , \tag{49}$$

and a break frequency of

$$\omega_c = \alpha_c(1 + Q_{m,c})^{1/2} . \tag{50}$$

Combining Equations 49 and 50 and solving for α_c yields

$$\alpha_c = \omega_c(1 - \gamma_{c,o})^{1/2} . \tag{51}$$

Therefore, if the coherence function is known, the prompt neutron decay constant, α_c, can be determined.

In the general and more realistic case where the detector efficiencies are not assumed to be equal, Equations 31 and 41 yield

$$\gamma(\omega,\$) = \left[\frac{Q_{x,m,c} \cdot Q_{y,m,c}}{[(1-\$)^2 + Q_{x,m,c} + (\omega/\alpha_c)^2][(1-\$)^2 + Q_{y,m,c} + (\omega/\alpha_c)^2]} \right]^{\frac{1}{2}} . \tag{52}$$

For a critical reactor \$=0 and the coherence function becomes

$$\gamma_c(\omega) = \left[\frac{Q_{x,m,c} \quad Q_{y,m,c}}{[1 + Q_{x,m,c} + (\omega/\alpha_c)^2][1 + Q_{y,m,c} + (\omega/\alpha_c)^2]} \right]^{1/2} . \tag{53}$$

The plateau value of the coherence function is now given by

$$\gamma_{c,o} = \gamma_c(\omega << \alpha_c) = \left[\frac{Q_{x,m,c} \quad Q_{y,m,c}}{(1 + Q_{x,m,c})(1 + Q_{y,m,c})} \right]^{1/2} , \tag{54}$$

and the break frequency is given by

$$\omega_c = \frac{(Q_{x,m,c} \quad Q_{y,m,c})^{1/4}}{\gamma_{c,o}^{1/2}} \alpha_c . \tag{55}$$

For the determination of α_c in this case Equations 54 and 55 are not sufficient and a third measured quantity along with $\gamma_{c,o}$ and ω_c is required which contains a relationship between $Q_{x,m,c}$ and $Q_{y,m,c}$. From Equation 33,

$$\frac{Q_{x,m,c}}{Q_{y,m,c}} = \frac{W_x D/R\beta^2}{W_y D/R\beta^2} = \frac{W_x}{W_y} , \tag{56}$$

and from Equation 14 and 16,

$$\frac{\bar{I}_x}{\bar{I}_y} = \frac{W_x \bar{q}_x n/\bar{\nu}\ell}{W_y \bar{q}_y n/\bar{\nu}\ell} = \frac{W_x \bar{q}_x}{W_y \bar{q}_y} . \tag{57}$$

If the detectors are of the same kind then $\bar{q}_x = \bar{q}_y$ and

$$\frac{\bar{I}_x}{\bar{I}_y} = \frac{W_x}{W_y} \quad . \tag{58}$$

Combining Equations 56 and 58, we have

$$r = \frac{\bar{I}_x}{\bar{I}_y} = \frac{W_x}{W_y} = \frac{Q_{x,m,c}}{Q_{y,m,c}} \quad . \tag{59}$$

Thus the ratio r, of the two mean currents $\bar{I}_x$ and $\bar{I}_y$, of the two detectors x and y can be used as the third measured quantity along with $\gamma_{c,o}$ and ω_c to determine α_c. Equations 54, 55 and 59 represent three equations and three unknowns, α_c, $Q_{x,m,c}$ and $Q_{y,m,c}$. Solving for these three unknowns, we have

$$Q_{y,m,c} = \frac{\gamma_{c,o}^2(1+r) + [\gamma_{c,o}^4(1+r)^2 + 4r\gamma_{c,o}^2(1-\gamma_{c,o}^2)]^{1/2}}{2r(1 - \gamma_{c,o}^2)} \quad , \tag{60}$$

$$Q_{x,m,c} = r\, Q_{y,m,c} \quad , \tag{61}$$

and

$$\alpha_c = \frac{\omega_c \gamma_{c,o}^{1/2}}{(Q_{x,m,c} \cdot Q_{y,m,c})^{1/4}} \quad . \tag{62}$$

IV. SHUTDOWN REACTIVITY FROM THE COHERENCE FUNCTION

A. Case of Identical Detectors

Seifritz [29] suggests that, besides the measurement of prompt neutron decay constant of the delayed critical reactor, the coherence function measurement offers a convenient possibility of subcriticality determination. From Equation 47 it is seen that the low-frequency coherence function is strongly dependent on the reactivity of the system. If one assumes, for simplicity, that the two neutron detectors have equal efficiencies ($W_x = W_y = W$), the subcritical reactivity yields with the use of Equations 47 and 48,

$$\$(\gamma_{c,o}, \gamma_{s,o}) = 1 - \left(\frac{\gamma_{c,o}}{1-\gamma_{c,o}} \frac{1-\gamma_{s,o}}{\gamma_{s,o}} \right)^{1/2}, \qquad (63)$$

where $\gamma_{c,o}$ and $\gamma_{s,o}$ are the plateau values of the coherence function for the critical and subcritical reactor respectively, and the reactivity, $\$ \leq 0$, is in dollars. The derivation of Equation 63 is given in Appendix D.

B. Case of Non-Identical Detectors

If the detector efficiencies are not equal, the relationship between the reactivity and the two plateau values given in Equation 63 will additionally contain the ratio of the

detector efficiencies given by Equation 59. From the general formulas for the subcritical and critical coherence functions given by Equations 52 and 53 and Equation 59 one can find the subcritical reactivity in this case as

$$\$(\gamma_{c,o}, \gamma_{s,o}, r) = 1 - \left\{ \gamma_{c,o} \frac{(1+r)\gamma_{c,o} + [(1-r)^2\gamma_{c,o}^2 + 4r]^{1/2}}{2r(1 - \gamma_{c,o}^2)} \right.$$

$$\left. \times \frac{[(1-r)^2\gamma_{s,o}^2 + 4r]^{1/2} - (1+r)\gamma_{s,o}}{2\gamma_{s,o}} \right\}^{1/2} . \qquad (64)$$

The derivation of this Equation is given in Appendix D.

C. Detection Efficiency Dependence of Subcriticality Measurements

It has been shown by Ackermann and Buhl [1] that a systematic error in the subcritical reactivity measurement may occur due to unexpected changes in the neutron detection efficiency. As was previously mentioned, the neutron detection efficiency, W, of a neutron detector placed in or near a reactor core is defined as the number of neutrons detected per fission occurring in the core. Ackermann and Buhl [1] give the following definition for detector efficiency as it is defined above:

$$W_n = \frac{\int_{V_d}\int_{\text{all E}} d\bar{r}dE\Sigma_d(\bar{r},E)\phi(\bar{r},E)}{\int_{V_c}\int_{\text{all E}} d\bar{r}dE\Sigma_f(\bar{r},E)\phi(\bar{r},E)}, \tag{65}$$

where V_d and V_c = detector and reactor core volumes, respectively

$\Sigma_d(\bar{r},E)$ and $\Sigma_f(\bar{r},E)$ = neutron detection and fission macroscopic cross reactions, respectively

$\phi(\bar{r},E)$ = space- and energy-dependent neutron flux.

W_n is very sensitive to a local perturbation in the flux distribution since the numerator is integrated in space only over the volume of the detector, whereas the denominator is integrated over the entire reactor core.

If we assume that $W_x = W_y = W$, but do not assume that the detector efficiency is the same for the reactor being critical or subcritical, that is to say, if $W_c \neq W_s$ it could be shown (Appendix D) that the subcriticality is defined as

$$\$ = 1 - \left(\frac{W_s}{W_c}\,\frac{\gamma_{c,o}}{1-\gamma_{c,o}}\,\frac{1-\gamma_{s,o}}{\gamma_{s,o}}\right)^{1/2}. \tag{66}$$

Equation 66 suggests that in order to calculate subcriticality one needs to know the detector efficiencies both when the reactor is critical and when it is subcritical, and that just knowing the ratio of detector efficiencies at critical state

is not sufficient.

For the more general case of having two asymmetric detectors such that $W_x \neq W_y$, the relationship corresponding to Equation 66 is

$$\$ = 1 - \left\{ \frac{Q_{y,m,s}}{2\gamma_{s,o}} \left[[\gamma_{s,o}^2 (1-r_s)^2 + 4r_s]^{1/2} - \gamma_{s,o}(1+r_s) \right] \right\}^{1/2}, \tag{67}$$

where

$$Q_{y,m,s} = \frac{W_{y,s}}{W_{y,c}} \gamma_{c,o} \frac{(1+r_c)\gamma_{c,o} + [(1-r_c)^2 \gamma_{c,o}^2 + 4r_c]^{1/2}}{2r_c(1-\gamma_{c,o}^2)}, \tag{68}$$

$$r_c = \frac{W_{x,c}}{W_{y,c}}, \tag{69}$$

and

$$r_s = \frac{W_{x,s}}{W_{y,s}}. \tag{70}$$

The formulation of Equations 67 and 68 are also given in Appendix D.

The ratio $r_c = W_{x,c}/W_{y,c}$ can be measured experimentally by the method outlined for deriving Equation 59. For measuring the ratio $r_s = W_{x,s}/W_{y,s}$ experimentally for the subcritical reactor, we can use Equation 14

$$\bar{I} = \frac{\varepsilon \bar{q} n}{\ell} \tag{71}$$

where ε = fraction of all neutrons absorbed in the reactor which are absorbed by the detector.

Now, in a subcritical reactor there is always a neutron source introduced to maintain a steady power level. Thus, ε can be defined in this case as

ε = [fraction of (neutrons produced by fission + neutrons emitted by the source) which are absorbed by the detector]

= [fraction of $(F\bar{\nu} + S)$ which are absorbed by the detector]

where

F = fission rate, and

S = neutron source strength.

It is also true that

Neutrons detected per second = $\varepsilon(F\bar{\nu} + S)$

= WF

Thus

$$\varepsilon = \frac{WF}{F\bar{\nu}+S} , \tag{72}$$

and

$$\bar{I} = \left(\frac{WF}{F\bar{\nu}+S}\right) \bar{q} \frac{n}{\ell} , \tag{73}$$

or

$$r_s = \frac{W_{x,s}}{W_{y,s}} = \frac{\bar{I}_{x,s}}{\bar{I}_{y,s}} \tag{74}$$

if identical detectors are used.

The ratio $W_{y,s}/W_{y,c}$ appearing in Equation 68 is not easy to get at experimentally. Using Equation 73, we can write

$$\bar{I}_{y,s} = \frac{W_{y,s}F_s}{F_s\bar{\nu}+S}\ \bar{q}\ \left(\frac{n}{\ell}\right)_s \tag{75}$$

for the subcritical reactor, and

$$\bar{I}_{y,c} = \left(\frac{W_{y,c}F_c}{F_c\ \bar{\nu}}\right)\ \bar{q}\ \left(\frac{n}{\ell}\right)_c$$

$$= \frac{W_{y,c}\bar{q}}{\bar{\nu}}\ \left(\frac{n}{\ell}\right)_c\ , \tag{76}$$

for the delayed critical reactor, where it has been assumed that the source intensity is zero at delayed critical. It is obvious that a ratio of mean currents from the detectors can not be used to measure the ratio $W_{y,s}/W_{y,c}$, and additional information about fission rates, F_s and F_c, total reaction rates $(n/\ell)_s$ and $(n/\ell)_c$, and source intensity S, is needed.

V. MEASUREMENT OF THE COHERENCE FUNCTION

A. Polarity Correlation Method

In contrast to the traditional procedure of calculating the coherence function by measuring the three spectral densities in Equation 39, $\gamma(\omega)$ is determined directly by the method of polarity correlation introduced by Seifritz [29] and shown in Figure 2.

If $x(\omega,t)$ and $y(\omega,t)$ are two correlated neutron noise signals with vanishing means, passed through bandfilters with the center frequency ω, their normalized joint-probability density function is given by Seifritz [29] as

$$f_{\omega}(x,y) = \{2\pi\sigma_x(\omega)\sigma_y(\omega)[1 - \gamma^2(\omega)]^{1/2}\}^{-1} \times$$

$$\exp\left\{\frac{1}{2[1-\gamma^2(\omega)]}\left[\frac{x^2}{\sigma_x^2(\omega)} - 2\gamma(\omega) \times \right.\right.$$

$$\left.\left.\frac{xy}{\sigma_x(\omega)\sigma_y(\omega)} + \frac{y^2}{\sigma_y^2(\omega)}\right]\right\} , \qquad (77)$$

where $\gamma(\omega)$ is the coherence function of filtered signals $x(\omega,t)$ and $y(\omega,t)$, and $\sigma_x^2(\omega)$ and $\sigma_y^2(\omega)$ are the mean-square values, $\overline{x^2}(\omega,t)$ and $\overline{y^2}(\omega,t)$ of the two filtered signals.

The appropriate assumption made for the validity of the bivariate distribution of Equation 77 is that $x(\omega,t)$ and $y(\omega,t)$

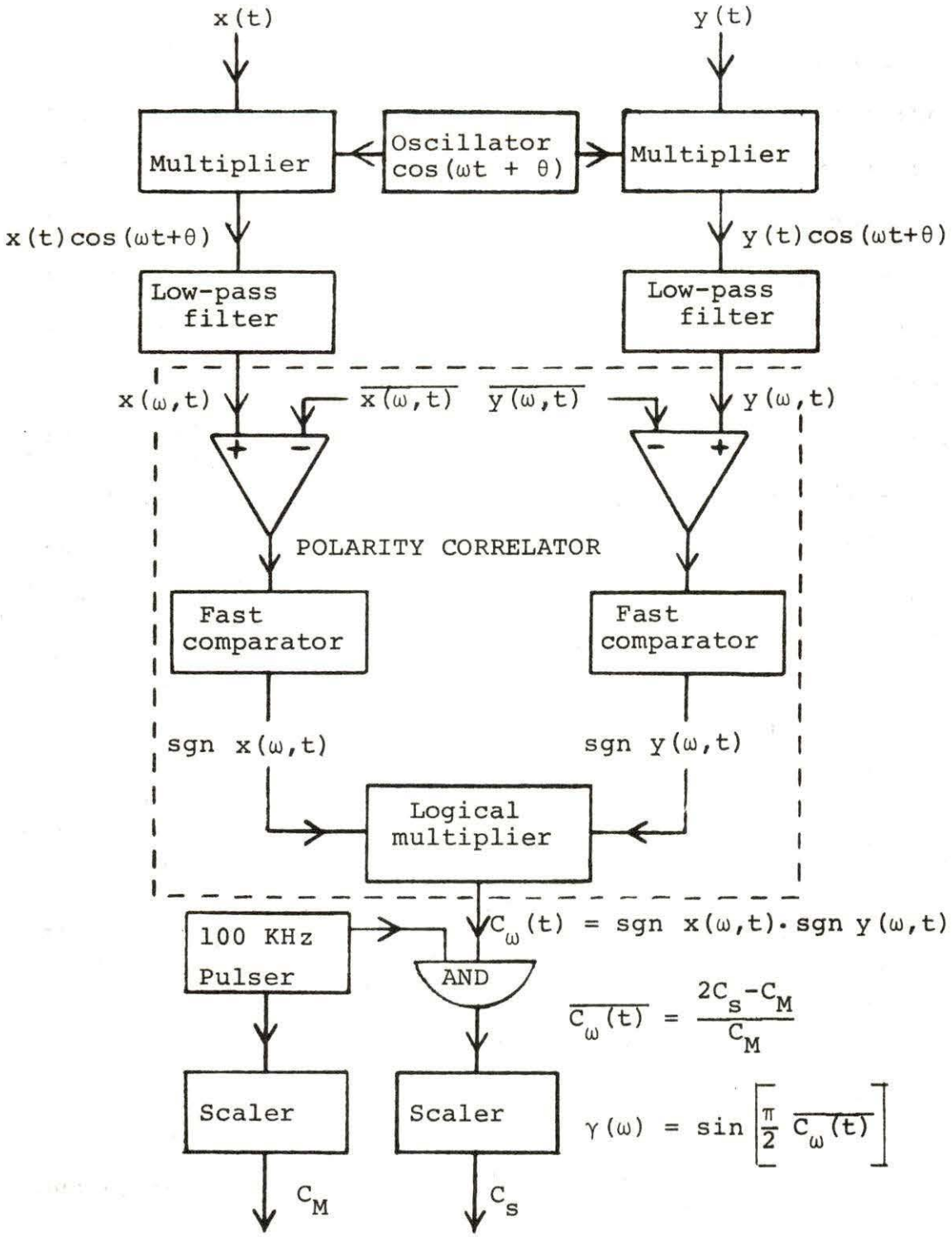

Figure 2. Block diagram of the polarity correlation technique in the frequency domain

are "normal random noise" signals.

It is clearly seen from the mathematical operations of the polarity correlator, indicated in Figure 2, that the coherence function $\gamma(\omega)$ is easily obtained by time averaging the correlator output $C_\omega(t)$. This signal is a binary random function with two logical states, +1 and -1. The upper state +1 and the lower state -1 are occupied if the signs of $x(\omega,t)$ and $y(\omega,t)$ coincide and anticoincide, respectively. The total probabilities P_+ and P_- that $C_\omega(t) = +1$ or -1 are given by the volumes enclosed between the probability surface $f_\omega(x,y)$ from Equation 77 and the plane x,y in the first and third quadrants or in the second and fourth quadrants. These probabilities derived by Cramer [12] are

$$P_+ = \int_0^\infty\int_0^\infty f_\omega(x,y)\,dxdy + \int_{-\infty}^0\int_{-\infty}^0 f_\omega(x,y)\,dxdy$$

$$= \frac{1}{2} + \frac{1}{\pi} \text{ arc sin } \gamma(\omega) \,, \tag{78}$$

and

$$P_- = \int_{-\infty}^0\int_0^\infty f_\omega(x,y)\,dxdy + \int_0^\infty\int_{-\infty}^0 f_\omega(x,y)\,dxdy$$

$$= \frac{1}{2} - \frac{1}{\pi} \text{ arc sin } \gamma(\omega). \tag{79}$$

Hence, the time averaged signal $C_\omega(t)$ is

$$\overline{C_\omega}(t) = P_+ - P_- = \frac{2}{\pi} \text{ arc sin } \gamma(\omega), \tag{80}$$

or the coherence function is obtained as

$$\gamma(\omega) = \sin\left[\frac{\pi}{2}\,\overline{C_\omega(t)}\right], \tag{81}$$

where $$\overline{C_\omega(t)} = \frac{C_s - (C_M - C_s)}{C_M}$$

$$= \frac{2C_s - C_M}{C_M} \quad , \tag{82}$$

where C_s is the "gated" scaler reading and C_M is the clock scaler reading, and the measurement is done for a specified period of time.

B. Dynamic Filtering

The filtering of the broadband noise signals can be achieved by means of dynamic filters as shown in Figure 2. The two signals x(t) and y(t) are multiplied by an oscillator signal, $\cos(\omega t+\theta)$. Since signals x(t) and y(t) may contain a spectrum of frequencies, the resulting output spectra will contain the sum and difference frequencies of every possible product of the frequency components of the two multiplied signals. If these resulting signals are passed through low pass filters, only the signals with frequencies equal to the difference of the oscillator frequency and components of the signal x(t) or y(t) which have a frequency $\omega_i \simeq \omega$ will get through. The above condition can be expressed as

$$\omega_i - \omega \lesssim \omega_b \ , \tag{83}$$

or

$$\omega - \omega_i \lesssim \omega_b \ , \tag{84}$$

where ω = oscillator frequency

ω_i = component i of input spectrum

ω_b = break frequency of low pass filter.

Since both conditions expressed in Equations 83 and 84 are sufficient for allowing a signal through the low pass filters, the effective width of the filters will be $2\omega_b$, centered around the frequency ω of the oscillator. By changing the oscillator frequency, the whole spectrum of the input signals can be scanned. The advantage of dynamic filtering is the better resolution $(\Delta\omega)/\omega$, which can be chosen independent of the center frequency ω.

The method of dynamic filtering is used to obtain coherence functions in this work. Adjustable band pass filters were used in subcriticality measurements.

C. Errors and Uncertainties

The variance in the measured value of the coherence function as defined by Equation 81 is given by Vaurio [35] as

$$\sigma^2(\gamma) = \frac{\pi^3}{\Delta\omega T}(1-\gamma^2)\left(1 - \frac{2}{\pi} \arcsin \gamma\right) \ , \tag{85}$$

where $\Delta\omega = 2\pi\Delta f$ is the width of band-pass filter used in the measurement, and T is the measurement time. It is obvious that to reduce the variance a long measurement time is necessary. This is achieved by recording the signals on magnetic tape for the desired time period, and then analyzing the recorded signal over the desired frequency range.

The variance for the value of subcriticality as given by Equation 63 can be calculated from Equation 85. Application of propagation of error analysis on Equation 63 gives

$$\sigma^2(\$) = \left(\frac{\partial \$}{\partial \gamma_{c,o}}\right)^2 \sigma^2(\gamma_{c,o}) + \left(\frac{\partial \$}{\partial \gamma_{s,o}}\right) \sigma^2(\gamma_{s,o}) \ , \qquad (86)$$

where

$$\left(\frac{\partial \$}{\partial \gamma_{c,o}}\right)^2 = \frac{(1 - \gamma_{s,o})}{4\gamma_{s,o}\gamma_{c,o}(1 - \gamma_{c,o})^3} \ , \qquad (87)$$

and

$$\left(\frac{\partial \$}{\partial \gamma_{s,o}}\right)^2 = \frac{\gamma_{c,o}}{4(1-\gamma_{c,o})(1-\gamma_{s,o})\gamma_{s,o}^3} \ . \qquad (88)$$

Equation 85 may be used to calculate $\sigma^2(\gamma_{c,o})$ and $\sigma^2(\gamma_{s,o})$, then Equation 86 takes the final form

$$\sigma^2(\$) = \frac{\pi^3}{4\Delta\omega T}\left[\frac{(1-\gamma_{s,o})(1+\gamma_{c,o})}{\gamma_{s,o}\gamma_{c,o}(1-\gamma_{c,o})^2}\left(1 - \frac{2}{\pi}\arcsin\gamma_{c,o}\right)\right.$$

$$\left. + \frac{\gamma_{c,o}(1+\gamma_{s,o})}{(1-\gamma_{c,o})\gamma_{s,o}^3}\left(1 - \frac{2}{\pi}\arcsin\gamma_{s,o}\right)\right] . \qquad (89)$$

It is evident from Equations 85 and 89 that to reduce uncertainties it is desirable to use as large a filter width as possible and as long a measurement time as feasible.

Korn and Korn [21] have given a definition for the variance of the coherence function as

$$\sigma^2(\gamma) = \frac{(1-\gamma^2)^2}{N} + 0(N^{-3/2}) , \qquad (90)$$

where N is the number of times the coherence function is sampled. This is simply the number of zero crossings in the present case where only the information carried in the polarity of the detector signal is used.

Bendat [5] gives the expected number of zero crossings in T seconds for band-limited white noise with zero lower-frequency cutoff as

$$N = \frac{0.577}{\pi}\ \omega_b T , \qquad (91)$$

where ω_b is the upper cutoff in radians per second. Since the coherence function is essentially a constant over the region of interest, Equation 91 may be used to evaluate N.

Hess and Albrecht [20] have used Equations 90 and 91 in conjunction with Equation 86 to derive an equation for the variance of the reactivity in dollars, which after making some corrections is given as

$$\sigma^2(\$) = \frac{1.361}{\omega_b T}\left[\left(\frac{1-\gamma_{s,o}}{1-\gamma_{c,o}}\right)\frac{(1+\gamma_{c,o})^2}{\gamma_{s,o}\gamma_{c,o}}\right.$$

$$\left. + \left(\frac{1-\gamma_{s,o}}{1-\gamma_{c,o}}\right)\frac{\gamma_{c,o}}{\gamma_{s,o}^3}(1+\gamma_{s,o})^2\right] . \qquad (92)$$

To arrive at Equation 92 the assumption was made that the lower-frequency cutoff was at zero. This assumption cannot be made for the present work due to the effect of delayed neutrons on the lower-frequency portion of the coherence function for the UTR-10 reactor. Band pass filters with lower frequency cutoff greater than zero were employed for subcriticality measurements for the UTR-10. Due to above reasoning, Equations 85 and 89 will be used for error analysis in this work. Equation 92 could be used if the effect of delayed neutrons are considered.

VI. EQUIPMENT AND PROCEDURES

Coherence function measurements were performed in the UTR-10 reactor at four different positions shown in Figure 3. All measurements but one were performed at a reactor power of 1 watt. One extra measurement was performed at position 1 at a power of 3 watts to study the effect of power level on the coherence function measurement. At position 1, an 8" x 4" x 4" piece of graphite was removed from the reactor so that the detectors could be inserted. At position 2 in the thermal column, a 50" x 4" x 4" piece of graphite was removed. At position 3 in the thermal column, an additional 19.5" piece of graphite had to be removed. At position 4 in the internal reflector of the reactor, the detectors were lowered in from the top of the reactor, after a 48" x 4" x 4" piece of graphite was removed and a 20" x 4" x 4" piece was put in place of it. The detectors were placed on top of this 20" stringer. At positions 2, 3 and 4, the detectors were placed in holes inside a 10" long piece of graphite which was locally fabricated. The holder kept the detectors in position and compensated for some of the removed graphite.

Equation 85 was used to determine length of measurement time necessary. It was decided that a 60 minute signal recording time was adequate. All coherence function measurements were made for 60 minutes except for the case of the 3 watt run at position 1, where a 90 minute recording time was

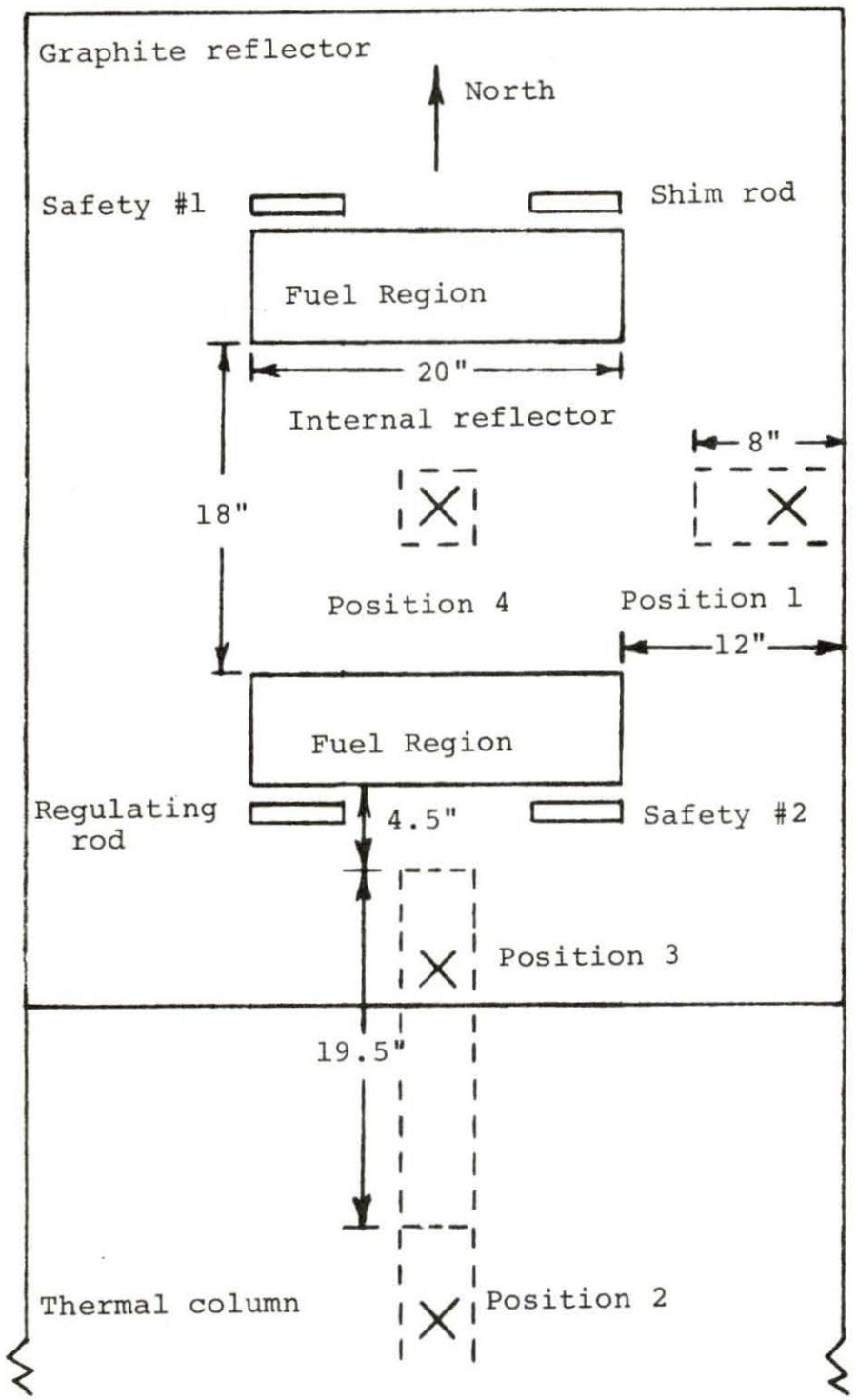

Figure 3. Detector positions 1, 2, 3 and 4, and control rod positions in the UTR-10 reactor

used.

The data acquisition system is shown in a block diagram in Figure 4. Two Westinghouse type 6376 fission chambers were placed side by side in the desired position in the reactor. The resulting currents from the fission chambers were fed to two high speed picoammeters (Keithley, model 417). The steady currents were suppressed and the fluctuations on top of the steady currents were amplified and converted to voltage signals. The resulting voltage fluctuations were then amplified on the TR-48 analog computer and recorded on two separate channels of an FM tape recorder (Precision Instrument, model PI-6200). The recording was done at a speed of 3.75 ips, and the recorded signals were monitored on a dual beam oscilloscope.

The block diagram of the data analysis system is given in Figure 2. The two signals $x(t)$ and $y(t)$ are the recorded data on tape which were played back at ten times the recording speed, i.e., at 37.5 ips, to shorten the analysis time. The process of playing back the recorded signal at ten times the recording speed multiplies all frequencies by a factor of 10. The analysis was then done at this higher frequency and the results were then adjusted to the original frequency. The signals $x(t)$ and $y(t)$ were multiplied by a common oscillator sinusoidal signal. The multiplication was performed on the TR-48 analog computer. The resulting signals were then fed to two band-pass filters (Krohn-Hite, model 330A), which were

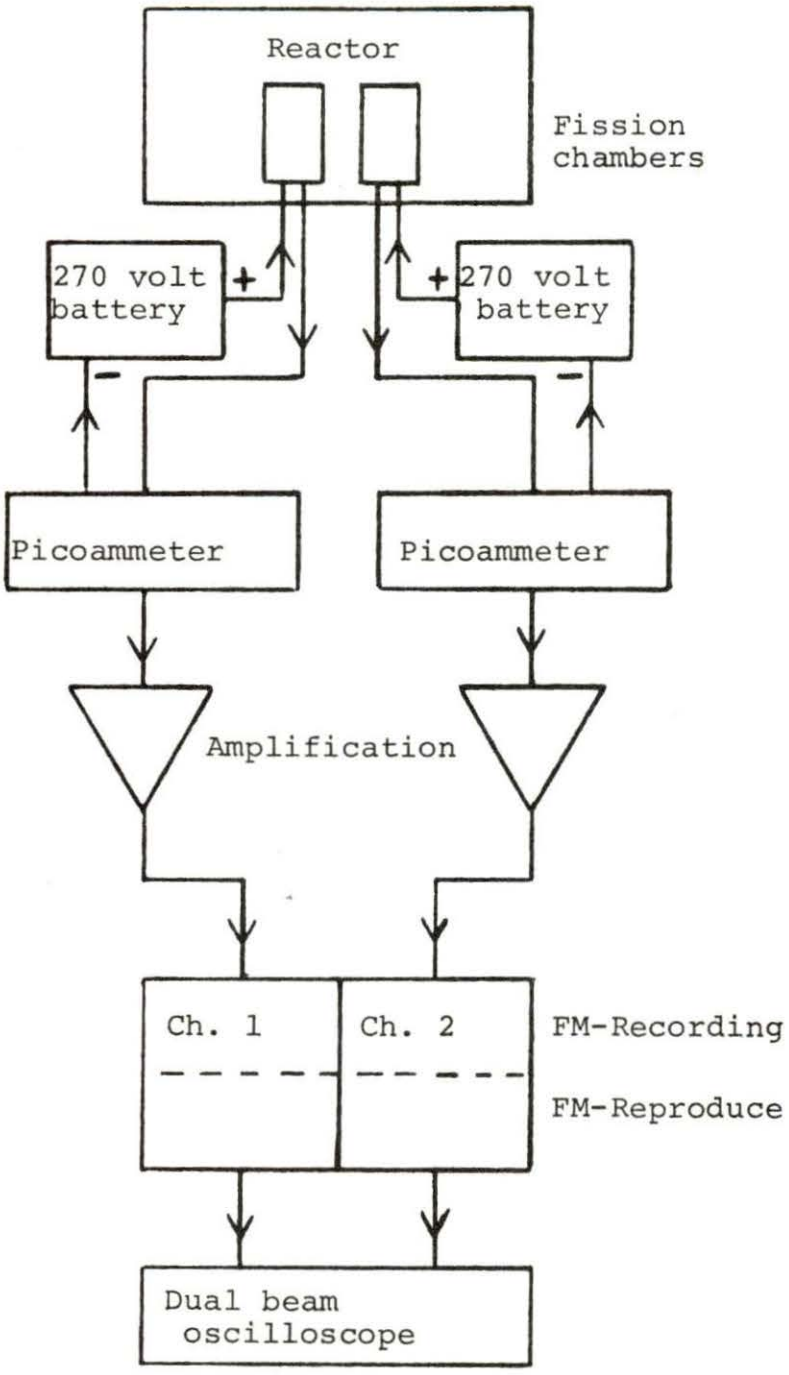

Figure 4. Data acquisition system

operated as low-pass filters by setting the low cutoff frequencies at their minimums (0.019 Hz). The outputs of the filters were then fed to the polarity correlator.

As was mentioned in the theory of polarity correlation, the two signals to be correlated need to have zero means. This requirement was achieved effectively by subtracting the mean value of the two signals from the signals as is shown schematically in Figure 2. To achieve this the two signals sgn $x(\omega,t)$ and sgn $y(\omega,t)$ shown in Figure 2 were taken directly to the AND gate and adjustments were made in the values of $\overline{x(\omega,t)}$ and $\overline{y(\omega,t)}$ until the gated scaler reading was one-half the clock scaler reading.

The output of the polarity correlator was used to gate a nuclear counter (Canberra, model 895) which was driven by a 100 KHz pulser. Another nuclear counter was used to record the number of pulses.

The oscillator frequency was changed over the desired frequency range and the coherence function was measured at specific frequencies. It was necessary to change the width of the filters at different center frequencies. The change was not made for all frequencies, rather a filter width was used for a specific frequency range.

The cutoff frequencies of the two filters were compared by feeding a sinusoidal test voltage to the filters and observing the Lissajous' patterns of the output voltage wave-

forms on a dual beam oscilloscope. The cutoff frequencies of the two filters were adjusted until a zero phase shift between the output signals of the two filters was observed.

The polarity correlator was locally constructed using the concepts provided by Lehto et al. [23].

From Equation 59, it is obvious that the ratio of the detector efficiencies could be measured experimentally by measuring the ratio of the average currents from the detectors. This could be done satisfactorily by measuring the ratio of the suppress currents on the picoammeters. To make sure that the suppress current readings on the picoammeters were equal to the input steady currents a picoampere source (Keithley, model 261) was used to feed known currents to the picoammeters, and the suppress currents which gave zero meter readings were recorded. It was found that the suppress currents were very nearly equal (within $\pm$ 0.5%) to input test currents.

As shown in Figure 2, the time average value $\overline{C_{\omega}(t)}$ was calculated using Equation 82, where C_s and C_M were read from the two nuclear counters. The value of the coherence function at each specific frequency was calculated using Equation 81. After measuring the coherence function over the desired frequency range, a logarithmic plot of the coherence function versus frequency was made and the plateau value γ_o and the break frequency ω_c were estimated from the plot. The ratio of the detector efficiencies, r, was also measured experimentally

by measuring the ratio of the suppress currents from the pico-ammeters. The application of values of γ_o, ω_c and r in Equations 60, 61 and 62 gives values for $Q_{x,m,c}$, $Q_{y,m,c}$ and α_c. These last three parameters and experimentally determined values of the coherence function at different frequencies were used to make a weighted least-squares fit to the coherence function given by Equation 53. The method of fitting used is that of Bevington [7], which is a least-squares fitting routine by linearization of the fitting function. The standard deviations of the coherence function at each frequency measured given by Equation 85, were used for weighting the least-squares fit.

To measure the subcritical reactivity, only the plateau values of the coherence function in the delayed critical and desired subcritical states were needed. Band-pass filters were used to analyze the data, and they were set over the flat (plateau) region of the coherence function.

The subcritical measurements were done directly without having to resort to recording the data on tape.

Equations 63 and 64 were used to calculate the sub-critical reactivity. The standard deviation in the measured subcriticalities were calculated from Equation 89.

In all coherence function measurements the cables from and to the detectors, the detectors, and the DC power supply for the detectors were shielded to reduce extraneous noise input.

VII. DISCUSSION AND RESULTS

A. Coherence Function Measurements

The results of coherence function measurements are given in Figures 5 through 9 for the five cases examined. The results of prompt neutron decay constant measurements are given in Table 1. They range from $\alpha_c = 42.6(\text{sec})^{-1}$ to $\alpha_c = 48.2(\text{sec})^{-1}$. The measurements agree very well with data of another investigator [9], who suggests $\alpha_c = 43.0(\text{sec})^{-1}$. The reactor manufacturer suggests a prompt neutron lifetime of $\ell = 1.35 \times 10^{-4}$ sec for the UTR-10 reactor. Assuming a delayed neutron fraction of $\beta = 0.0064$, we have $\alpha_c = \beta/\ell = 47.4(\text{sec})^{-1}$.

The value of $\alpha_c = 48.2(\text{sec})^{-1}$ deviates from the average of all measurements ($\alpha_c = 44.4(\text{sec})^{-1}$) more than other values. A reason for this could be that the detectors were nearest to the core for this case. Since prompt neutron lifetime is shorter in light water than it is in graphite, a larger value of α_c is expected at or near the core.

The plateau value of the coherence function, γ_o, is largest when the signal-to-noise ratio (S/N) is the largest, which agrees with Equation 54. The break frequency, ω_c, changes from 55.1 to 111 sec^{-1} in the cases examined. The reason is quite visible from the form of Equation 55, which shows that the break frequency will increase as S/N increases. It must be noted that the break frequency of the coherence

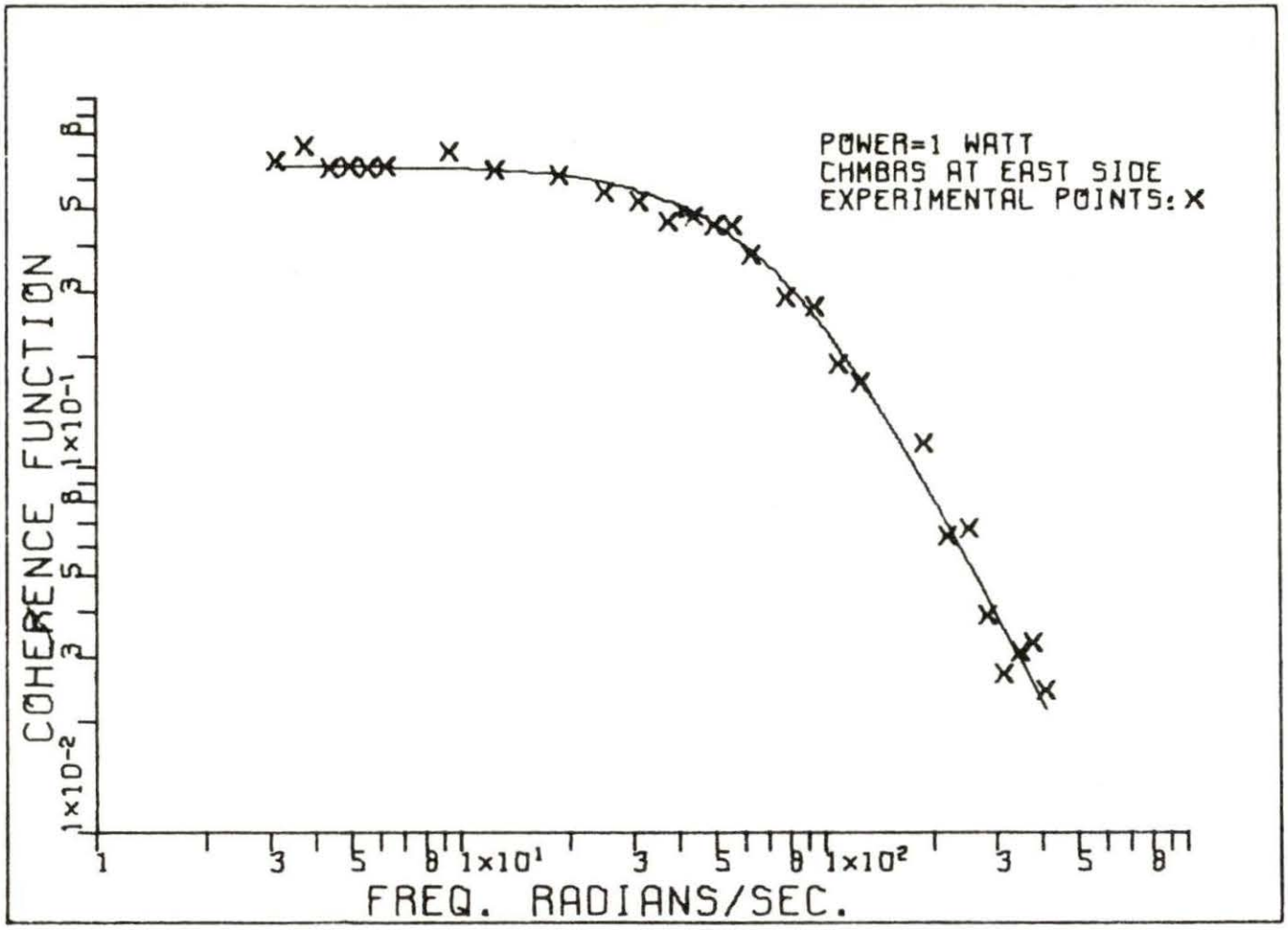

Figure 5. Coherence function at position 1 and power of 1 watt

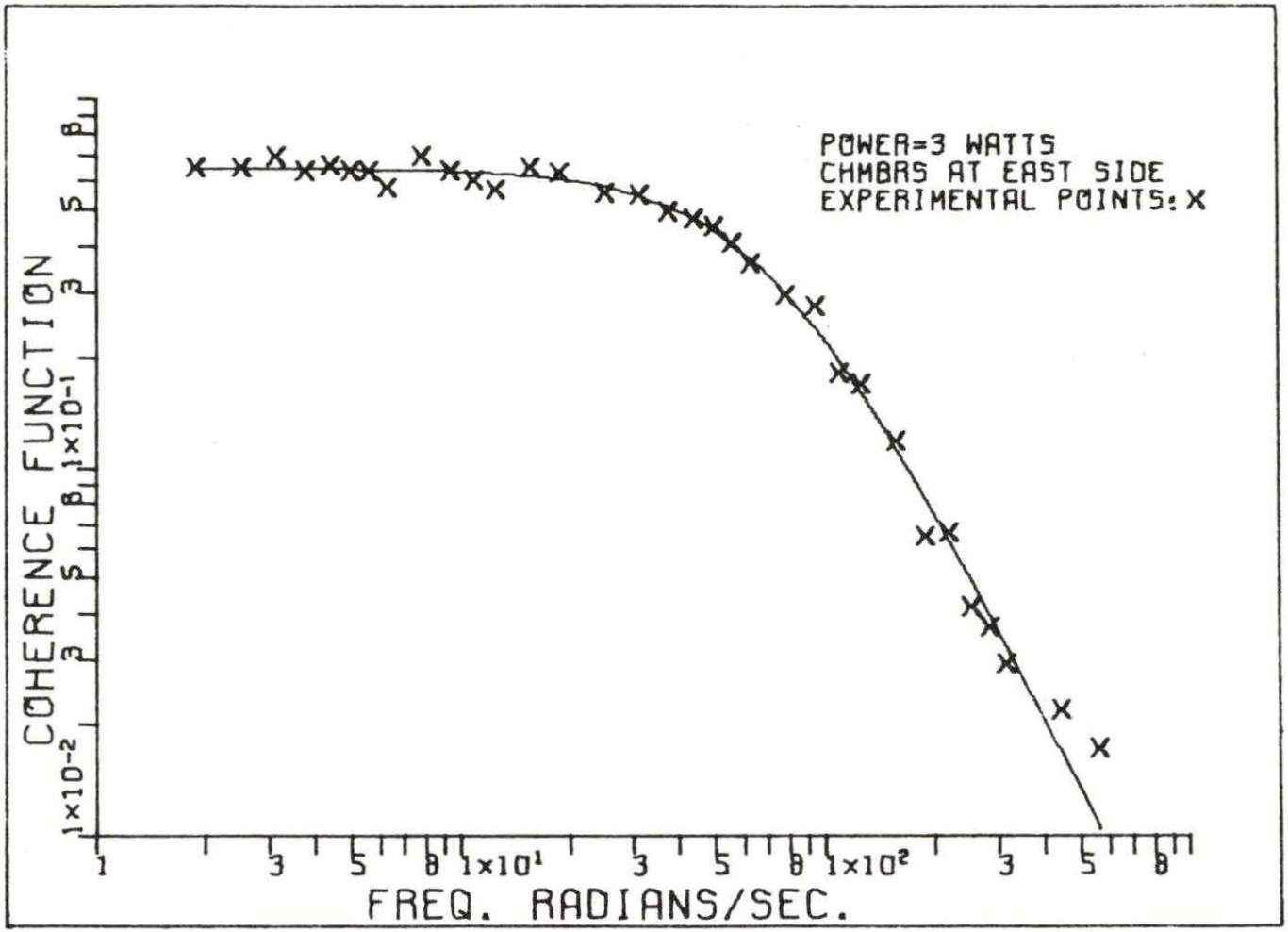

Figure 6. Coherence function at position 1 and power of 3 watts

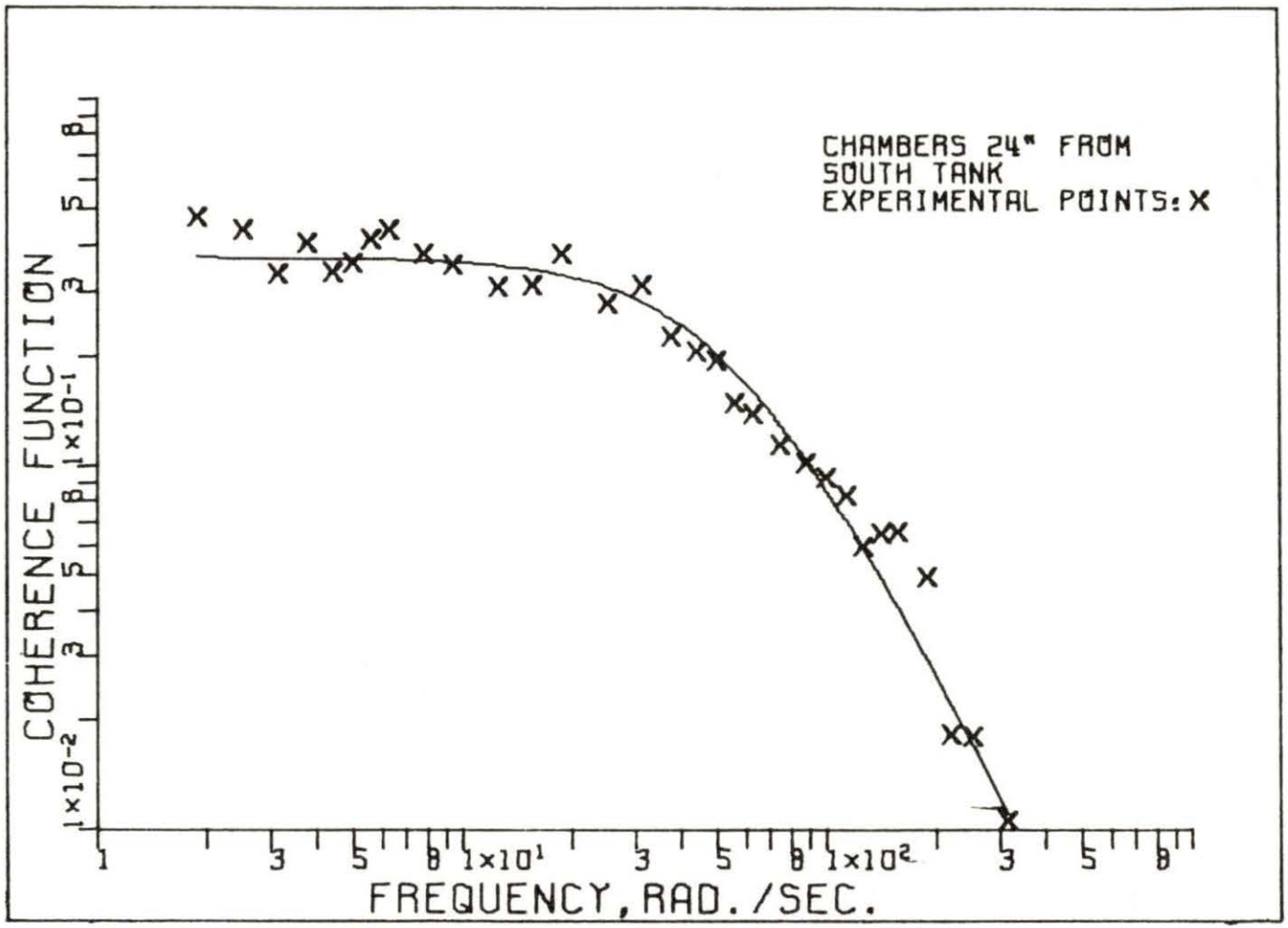

Figure 7. Coherence function at position 2

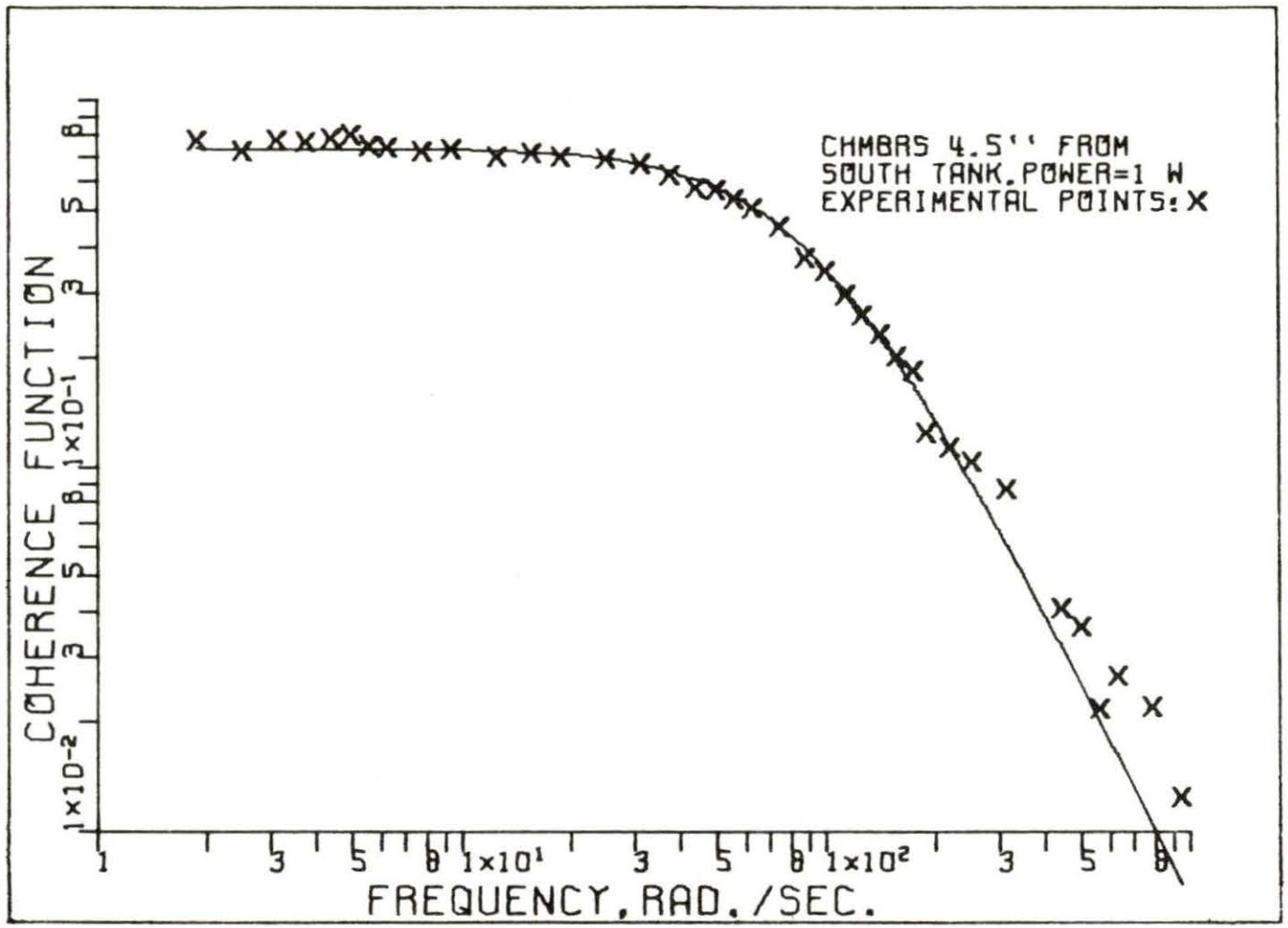

Figure 8. Coherence function at position 3

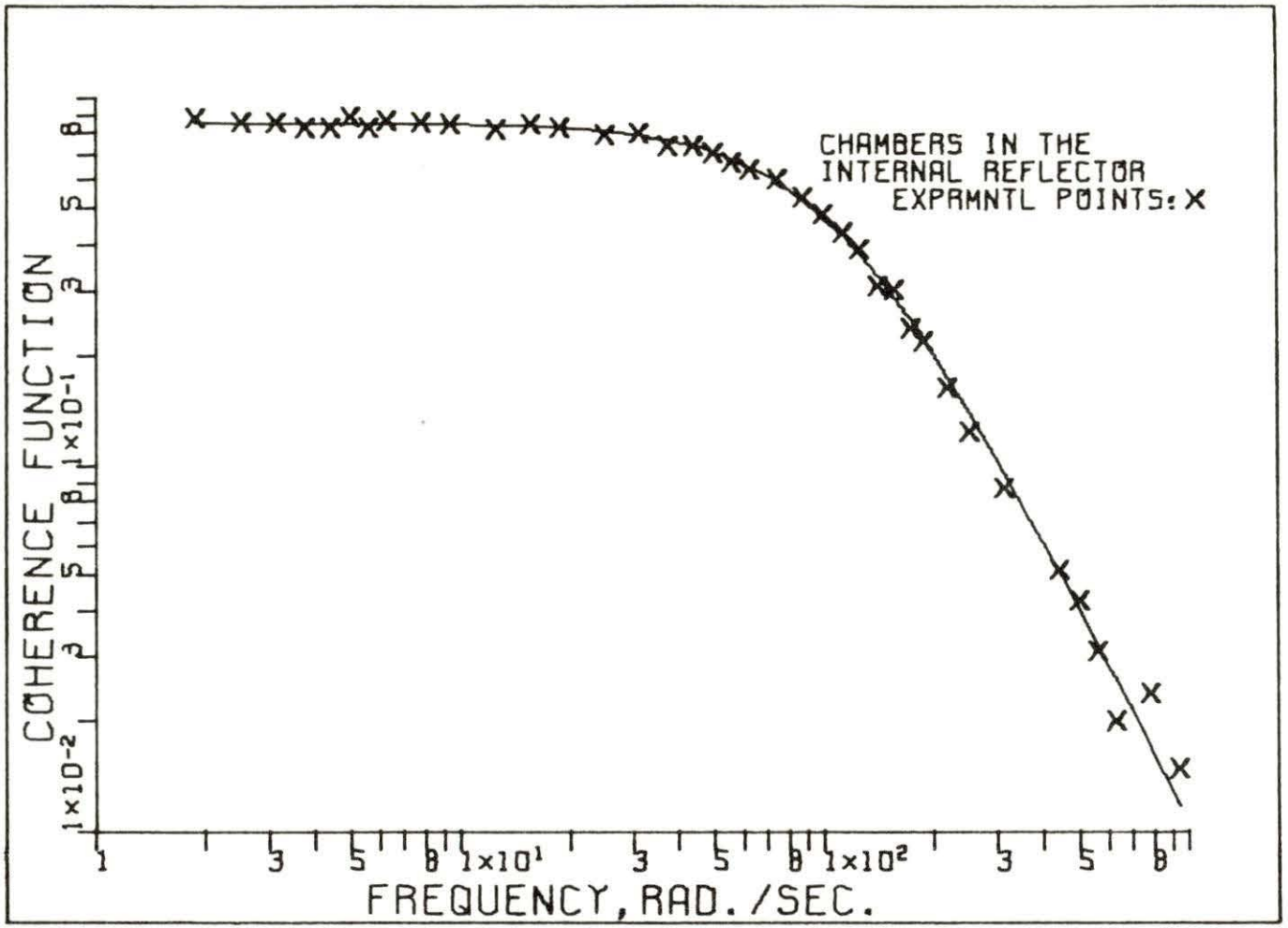

Figure 9. Coherence function at position 4

Table 1. Results of $\alpha_c = \beta/\ell$ measurements in the UTR-10 reactor

	$r = \frac{\bar{I}_x}{\bar{I}_y}$	$Q_{x,m,c}$	$Q_{y,m,c}$	$\frac{Q_{x,m,c}}{Q_{y,m,c}}$	$\alpha_c=\beta/\ell$ sec^{-1}	ω_c sec^{-1}	γ_o	W_x $\times 10^4$	W_y $\times 10^4$
Detectors at position 1, power = 1 watt	1.02	2.10	1.72	1.22	44.2	75.4	0.655	1.29	1.06
Detectors at position 1, power = 3 watts	1.05	1.84	1.80	1.02	43.0	72.2	0.645	1.13	1.10
Detectors at position 2, power = 1 watt	1.04	0.63	0.548	1.15	43.8	55.1	0.370	0.387	0.337
Detectors at position 3, power = 1 watt	1.06	2.97	2.66	1.12	48.2	94.0	0.737	1.82	1.63
Detectors at position 4, power = 1 watt	1.04	5.91	5.76	1.03	42.6	111	0.854	3.63	3.54

function is directly proportional to the prompt neutron decay constant. In fast reactors where the prompt neutron decay constant is large the break frequency occurs at much higher frequencies ($\sim 10^4$ sec^{-1}), as could be seen from the results obtained by Seifritz [29]. In the UTR-10, which is a light water moderated and graphite reflected reactor, some moderation is also done by the graphite, and the value of α_c is expected to be lower than what one might observe in a light water moderated and reflected reactor.

The above effect influences the measurement of α_c by the coherence function method since as it is suggested by Yasuda and Miyoshi [36] the mean lifetime of precursors of the short-lived delayed neutron emitters is not sufficiently longer than the lifetime of prompt neutrons in a reactor like UTR-10. This complicates separation of the prompt neutron decay mode from the associated delayed neutron decay mode. To demonstrate this effect for the UTR-10 reactor, a "theoretical" coherence function was developed, given in Appendix E, which takes into account the effect of delayed neutrons. The resulting coherence function was plotted on logarithmic paper, and the fitted coherence function measured at 3 watts was superimposed on this "theoretical" curve for comparison purposes. The result is given in Figure 10. It can be seen that the effect of the delayed neutrons is quite pronounced, and possibly affects the break frequency determination, and hence the

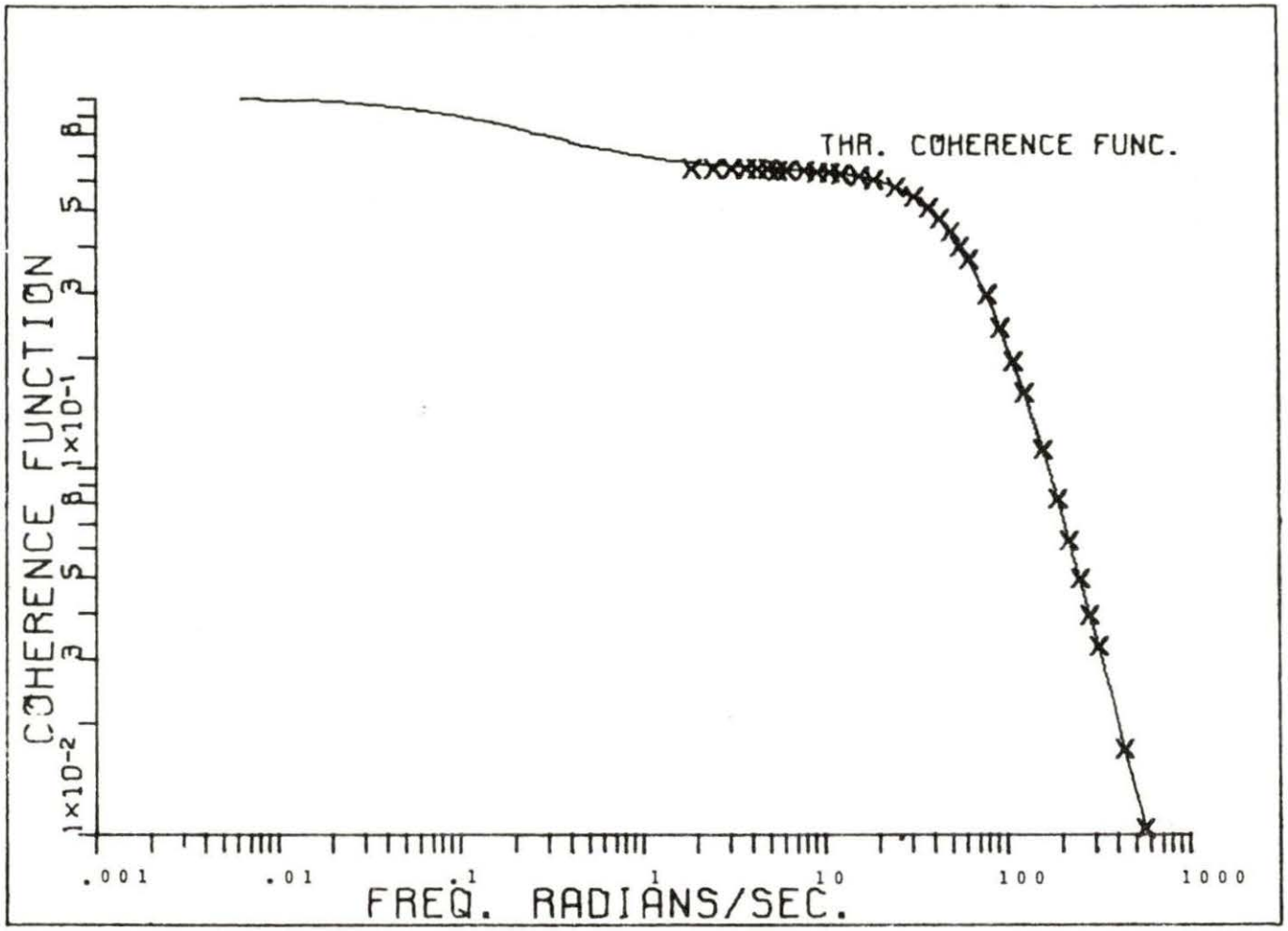

Figure 10. Theoretical coherence function compared with curve-fitted coherence function at 3 watts (X)

measured value of α_c. It should also be noted that some graphite had to be removed from the reactor during each coherence function measurement, which had some effect on the results, since the composition of the reactor was slightly altered in each case. The most important case is probably the removal of some graphite from the internal reflector of the reactor.

The detector efficiencies given in Table 1 were calculated using Equation 33 and a Diven factor equal to 0.8 for pure U^{235}, a Bennett factor of 1.2, and a delayed neutron fraction of 0.0064.

The results of the coherence function measurements at 4.5" from the south tank are given in Appendix F.

B. Subcritical Reactivity Measurements

During the normal operation of the UTR-10 reactor the two safety rods shown in Figure 3 are fully withdrawn and the positions of the shim rod and regulating rod are adjusted to achieve criticality at desired power level. To operate the reactor at a subcritical state, the shim and regulating rods could be inserted and a source of neutrons introduced so that a constant power level could be maintained. The two safety rods could subsequently be inserted to give different states of subcriticality.

Table 2 summarizes the results of subcriticality measurements at three positions in the UTR-10 reactor. Three states of subcriticality were examined for each position, except for position 3, where a fourth configuration was also examined. In the case that shim and regulating rods are fully inserted but the safety rods are kept withdrawn, the subcriticality can be calculated approximately from the rod worth curves of the reactor. This information is also given in Table 2. Also an average of subcriticality values measured in the north and south cores of the UTR-10, using pulsed neutron source technique and Gozani method of calculation [18] are given for comparison. It must be noted that the pulsed neutron technique of measuring subcriticality is space dependent. The standard deviation values and the per cent standard deviation values were calculated using Equation 89.

As can be seen from Equation 89 the variance of the subcriticality values can be reduced by increasing the measurement time. A measurement time of 20 minutes was used for all subcriticalities given in Table 2. The standard deviations are large because a very narrow filter width of 0.7 Hz (0.7 - 1.4 Hz) had to be used. The reason for choosing such a narrow filter width can be seen from Figure 10. Both the effect of delayed neutrons and low break frequency decrease the width of the plateau region of the coherence function over which the band filters could be set. For a ^{239}Pu fueled fast reactor

Table 2. Subcriticalities ($), standard deviations ($\sigma_{\$}$) and per cent standard deviations ($\%\sigma_{\$}$), all given in dollars, for 3 detector positions and 4 reactor configurations

	Detectors at position 1, east side of the reactor			Detectors at position 3, 4-1/2 inches from south tank			Detector at position 4, in the internal reflector			Subcriticalities by pulsed neutron technique
	$	$\sigma_{\$}$	$\%\sigma_{\$}$	$	$\sigma_{\$}$	$\%\sigma_{\$}$	$	$\sigma_{\$}$	$\%\sigma_{\$}$	$(GOZ)
Safety #1 and 2 out (Case 1)	-0.769	0.280	36.4	-0.599	0.224	37.4	-1.06	0.282	26.6	-0.95
Safety #1 and 2 out, from rod worth curves	-0.55	--	--	-0.53	--	--	-0.75	--	--	--
Safety #2 out (Case 2)	--	--	--	-1.09	0.329	30.2	--	--	--	--
Safety #1 out (Case 3)	-2.59	1.17	45.2	-2.67	0.97	36.3	-2.40	0.583	24.3	-2.14
Rods in (Case 4)	-3.89	2.72	69.9	-3.85	1.94	50.4	-3.81	2.99	78.5	-2.99

the break frequency is at a much higher frequency. Here a filter width of ∿100 Hz could be used [29], which reduces the variance in the values of measured subcriticalities. The other alternative in the present case was to increase measurement time considerably. This was found to be impractical.

As was shown by Equation 65 the detector efficiencies depend on their position in the reactor and hence the flux at that position. It can also be seen from Equation 66 that the subcriticality is dependent on the value of detector efficiency at the subcritical state as well as the critical state. The subcriticality measurements at the three positions given in Table 2 were performed for a set of identical rod positions so that the effect of position dependence could be studied. This effect is quite visible in the data of Table 2. Particularly for position 3 where the detectors were in the vicinity of the regulating rod and safety rod #2, the effect can be seen for cases 2 and 3 given in Table 2. In each case both the shim and regulating rods were inserted, but for case 2 safety rod #1 was also inserted, while for case 3 safety rod #2 was inserted. Although the two safety rods are supposedly of the same worth, the subcriticality in the case 3 was lower than case 2 due to the fact that the flux was lowered at the detector position by inserting safety rod #2.

VIII. SUMMARY AND CONCLUSIONS

It was demonstrated in the theoretical part of this work that the coherence function is independent of uncorrelated input noise and the frequency response of the signal analysis system. It was pointed out that the theory of polarity correlation applied only to zero mean value signals, thus making it necessary to adjust signals with non-zero means before they were processed by the polarity correlator.

Coherence function measurements and subcritical reactivity measurements were made at different positions in the UTR-10 reactor. Prompt neutron decay constants were calculated for each position from the coherence function. Based on the results of these measurements the following conclusions can be made:

1. The value of prompt neutron decay constant does not change with the position of the detectors except for the case of detectors being closest to the fuel region where a larger value is observed. This larger value is probably due to the fact that prompt neutron lifetime is lower in water than it is in graphite.

2. Subcritical reactivity measurements are dependent on the position of the detectors as was expected from the theory presented.

3. In a reactor like the UTR-10, where some moderation is done by graphite, the break frequency of the coherence

function occurs at frequencies less than ∿110 rad/sec. This effect dictates the use of narrow filter band widths in subcriticality measurements which in turn reduces the precision of these measurements.

IX. SUGGESTIONS FOR FURTHER WORK

Some extensions could be made in the work presented here, in both theoretical and experimental aspects.

The theory could be extended by adding the effect of delayed neutrons and extraneous neutron sources to the derivation of the reactor noise source formula.

The theory of subcritical reactivity measurements can be extended by considering the effect of detector efficiency changes with local flux variations.

Compensation for detector efficiency changes could be applied if accurate measurements of source intensity, fission rate, and total reaction rate were available.

More precise subcriticality measurements are possible by increasing the measurement time and studying the effect of larger filter band widths.

Use of more efficient detectors like ^{3}He detectors can increase the precision of all measurements.

X. LITERATURE CITED

1. N. J. Ackermann and A. R. Buhl, Nuclear Technology, 12, 320 (1971).

2. R. Badgley and R. Uhrig, Nuc. Sci. Eng., 19, 158 (1964).

3. J. Balcomb in Noise Analysis in Nuclear Systems, Proceedings of the Symposium, Gainesville, Florida, 1963, pp. 183-201.

4. J. Balcomb, H. Demuth, and E. Gyftopoulous, Nuc. Sci. Eng., 9, 159 (1961).

5. J. S. Bendat, Principles and Applications of Random Noise Theory, pp. 1-143, Wiley and Sons, Inc., New York (1958).

6. J. S. Bendat and A. G. Piersol, Random Data: Analysis and Measurement Procedures, Wiley and Sons, Inc., New York (1971).

7. P. R. Bevington, Data Reduction and Error Analysis for the Physical Sciences, pp. 237-240, McGraw-Hill, New York (1969).

8. R. G. Brown and J. W. Nilsson, Introduction to Linear Systems Analysis, pp. 78-247, Wiley and Sons, Inc., New York (1962).

9. T. Chan, "Reactor Transfer Function Measurements with the Reactor Oscillator," M.S. Thesis, Iowa State University, (1971).

10. C. E. Cohn, Nuc. Sci. Eng., 5, 331 (1959).

11. C. E. Cohn, Nuc. Sci. Eng., 7, 472 (1960).

12. H. Cramer, Mathematical Methods of Statistics, pp. 287-290, Princeton University Press, Princeton, N.J. (1946).

13. R. A. Danofsky in Noise Analysis in Nuclear Systems, Proceedings of the Symposium, Gainesville, Florida, 1963, pp. 229-248.

14. J. B. Dragt in Neutron Noise, Waves, and Pulse Propagation, Transactions of the Symposium, Gainesville, Florida, 1966, pp. 47-48.

15. J. B. Dragt, Nukleonik, 8, 188 (1966).

16. S. Glasstone and A. Sesonske, Nuclear Reactor Engineering, pp. 297-298, D. VanNostrand, Princeton, New Jersey (1967).

17. S. Goldman, Frequency Analysis, Modulation and Noise, pp. 355-356, McGraw-Hill, New York (1948).

18. G. W. Hannaman, "Reactivity Measurements Based on the Pulsed Neutron Technique," M.S. Thesis, Iowa State University (1971).

19. R. A. Hendrickson, "Cross-Spectral Density Measurements in a Coupled-Core Reactor," Ph.D. Dissertation, Iowa State University (1966).

20. G. M. Hess and R. W. Albrecht, Trans. Am. Nucl. Soc., 12, 738 (1969).

21. G. A. Korn and T. M. Korn, Mathematical Handbook for Scientists and Engineers, p. 622, McGraw-Hill, New York (1961).

22. R. C. Kryter, D. N. Fry, and D. P. Roux, Trans. Am. Nuc. Soc., 10, 283 (1967).

23. W. Lehto, M. Larson, R. Goin and J. Hutton, Nuc. Ins. Meth., 97, 507 (1971).

24. N. Pacilio, Nuc. Sci. Eng., 35, 249 (1969).

25. V. Rajagopal, Nuc. Sci. Eng., 12, 218 (1962).

26. J. C. Robinson and N. J. Ackermann, Nuclear Technology, 13, 250 (1972).

27. D. P. Roux and A. R. Buhl, Nuclear Technology, 12 137 (1971).

28. M. A. Schultz, Control of Nuclear Reactors and Power Plants, 2 ed., pp. 85-132, McGraw-Hill, New York (1961).

29. W. Seifritz, Nuc. Appl. Tech., 7, 513 (1969).

30. W. Seifritz, D. Stegemann, and W. Vath in Neutron Noise, Waves, and Pulse Propagation, Transactions of the Symposium, Gainesville, Florida, 1966, p. 40.

31. J. R. Sheff and R. W. Albrecht, Nuc. Sci. Eng., 24, 246 (1966).

32. T. E. Stern in Noise Analysis in Nuclear Systems, Proceedings of the Symposium, Gainesville, Florida, 1963, pp. 203-215.

33. R. E. Uhrig, Random Noise Techniques in Nuclear Reactor Systems, pp. 83-119, Ronald Press, New York (1970).

34. J. Valat in Noise Analysis in Nuclear Systems, Proceedings of the Symposium, Gainesville, Florida, 1963, pp. 219-228.

35. J. K. Vaurio, Journal of Nuclear Energy, 26, 44 (1772).

36. H. Yasuda and R. Miyoshi, Nuc. Sci. Tech., 9, 40 (1972).

XI. ACKNOWLEDGMENTS

The author wishes to express his gratitude to his major professor, Dr. Richard A. Hendrickson. His tireless counsel and instructive advice during the investigation, and in preparing this thesis is highly appreciated.

A special appreciation is expressed by the author to his father, Mr. Mehdi Nabavian, whose financial support made this educational experience possible.

It is also a pleasure to express appreciation to the staff of the UTR-10 reactor for many hours of preparation and reactor operation during the experiment.

XII. APPENDIX A: REACTOR NOISE

SOURCE FORMULATION

This formulation follows the method given by Cohn [11].

The specific reactions contributing to the noise-equivalent source are listed in the following table.

Table A1. Contributions to pile noise source

Nature of process	Average rate of occurrence (q_i)	Net number of neutrons produced ($\bar{m}_i$)
Non-productive absorption including leakage	$\frac{n}{\ell} \frac{\Sigma_c}{\Sigma_c + \Sigma_f}$	-1
Fission giving rise to ν prompt neutrons	$\frac{n}{\ell} \frac{\Sigma_f}{\Sigma_c + \Sigma_f} P\nu$	ν-1

Here the only reactions considered are nonproductive absorption, leakage, and fission. Additional reactions comprising the generation and decay of delayed neutron precursors give contributions a fraction β weaker than the others, and thus are neglected. Here, Σ_c is the macroscopic cross reaction for all nonproductive neutron absorptions including leakage, Σ_f is the macroscopic cross reaction for fission, n is the total number of neutrons in the reactor, ℓ is the prompt neutron lifetime and β is the delayed neutron fraction. Σ_c and Σ_f are subject to the criticality condition

$$\bar{\nu}\Sigma_f/(\Sigma_c + \Sigma_f) = 1 \ , \tag{A1}$$

where $\bar{\nu}$ is the average number of neutrons, both prompt and delayed, produced per fission. P_ν is the probability that ν prompt neutrons will be produced in any one fission. It is subject to the constraints

$$\sum_{\nu=1}^{\infty} P_\nu = 1 \ , \tag{A2}$$

$$\sum_{\nu=1}^{\infty} \nu P_\nu = (1-\beta)\bar{\nu} \approx \bar{\nu} \ , \tag{A3}$$

$$\sum_{\nu=1}^{\infty} \nu^2 P_\nu \approx \overline{\nu^2} \ . \tag{A4}$$

Substitution of the quantities in Table A1 into the equation for the spectral density of the noise-equivalent source

$$\Phi_{ns} = 2 \sum_i q_i^2 \bar{m}_i \ , \tag{A5}$$

yields

$$\Phi_{ns} = \frac{2n}{\ell(\Sigma_c + \Sigma_f)} \left[\Sigma_c + \Sigma_f \sum_{\nu=1}^{\infty} (\nu-1)^2 P_\nu\right] \ . \tag{A6}$$

Application of the conditions A1, A2, A3, and A4 then yields

$$\Phi_{ns} = \frac{2n}{\ell} \quad \frac{\overline{\nu^2} - \bar{\nu}}{\bar{\nu}}$$

$$= \frac{2n\bar{\nu}D}{\ell} \qquad \text{(A7)}$$

where $$D = \frac{\overline{\nu^2} - \bar{\nu}}{\bar{\nu}^2} \qquad \text{(A8)}$$

is the Diven factor.

XIII. APPENDIX B: REACTOR OPEN LOOP TRANSFER FUNCTIONS FORMULATION

Following the procedures given by Glasstone and Sesonske [16], and Schultz [28], formulas are derived for source and reactivity transfer functions for both critical and sub-critical reactors for the case of one delayed neutron group.

The point reactor kinetic equations are

$$\frac{dn}{dt} = \frac{\delta k_o}{\ell} n - \frac{k_o \beta n}{\ell} + \lambda C + S \qquad \text{(B1)}$$

$$\frac{dC}{dt} = \frac{k_o \beta n}{\ell} - \lambda C \qquad \text{(B2)}$$

where

n = time dependent neutron density (neutrons/cm^3)

C = time dependent delayed neutron precursor concentration (cm^{-3})

k_o = neutron multiplication constant at steady state

$\delta k_o = k_o - 1$

β = one group delayed neutron fraction

λ = one group delayed neutron precursor decay constant (sec^{-1})

ℓ = prompt neutron lifetime (sec)

S = time dependent extraneous neutron source density (neutrons/sec-cm^3)

A. Source Transfer Function

To derive the source transfer function let

$$n = n_o + \delta n \tag{B3}$$

$$C = C_o + \delta C \tag{B4}$$

$$S = S_o + \delta S \tag{B5}$$

where n_o, C_o and S_o are quantities at time zero and δn, δC and δS represent small perturbations of time zero values.

Substituting Equations B3, B4 and B5 in Equations B1 and B2 we have

$$\frac{d}{dt}\,\delta n = \frac{\delta k_o n_o}{\ell} + \frac{\delta k_o \delta n}{\ell} - \frac{k_o \beta n_o}{\ell} - \frac{k_o \beta \delta n}{\ell} + \lambda C_o + \lambda \delta C + S_o + \delta S \tag{B6}$$

$$\frac{d}{dt}\,\delta C = \frac{k_o \beta n_o}{\ell} + \frac{k_o \beta \delta n}{\ell} - \lambda C_o - \lambda \delta C \tag{B7}$$

At steady state Equations B6 and B7 reduce to

$$0 = \frac{\delta k_o n_o}{\ell} - \frac{k_o \beta n_o}{\ell} + \lambda C_o + S_o \tag{B8}$$

$$0 = \frac{k_o \beta n_o}{\ell} - \lambda C_o \quad . \tag{B9}$$

Thus we have

$$\lambda C_o = \frac{k_o \beta n_o}{\ell} \, , \tag{B10}$$

and substituting in Equation B8 we have

$$S_o = - \frac{\delta k_o n_o}{\ell} \quad . \tag{B11}$$

Substituting back into Equations B6 and B7 and introducing new notations

$$\rho_o = (k_o - 1)/k_o \ , \tag{B12}$$

for time zero reactivity and

$$\Lambda = \ell/k_o \ , \tag{B13}$$

for neutron generation time we have

$$\frac{d}{dt}\,\delta n = \frac{\rho_o \delta n}{\Lambda} - \frac{\beta \delta n}{\Lambda} + \lambda \delta C + \delta S \tag{B14}$$

$$\frac{d}{dt}\,\delta C = \frac{\beta \delta n}{\Lambda} - \lambda \delta C \ . \tag{B15}$$

The Laplace transform of this coupled set of linear differential equations is

$$s\Delta N(s) = \frac{\rho_o}{\Lambda}\,\Delta N(s) - \frac{\beta}{\Lambda}\,\Delta N(s) + \lambda \Delta C(s) + \Delta S(s) \tag{B16}$$

$$s\Delta C(s) = \frac{\beta}{\Lambda}\,\Delta N(s) - \lambda \Delta C(s) \ . \tag{B17}$$

Solving for $\Delta C(s)$ in Equation B17 and substituting in Equation B16 we find the source transfer function

$$\frac{\Delta N(s)}{\Delta S(s)} = H_s(s) = \frac{1}{s - \frac{\rho_o}{\Lambda} + \frac{\beta}{\Lambda} - \frac{\lambda\beta}{\Lambda(s+\lambda)}} \ . \tag{B18}$$

Multiplying the numerator and denominator by $(s+\lambda)$, and assuming that $\lambda << (\rho_o - \beta)/\Lambda$, we have

$$H_s(s) = \frac{s+\lambda}{s^2 + \left[\frac{\beta-\rho_o}{\Lambda}\right]s - \frac{\rho_o\lambda}{\Lambda}} \quad . \tag{B19}$$

Substituting $s = j\omega$ and taking the square modulus of the transfer function, we have

$$|H_s(\omega)|^2 = \frac{\omega^2 + \lambda^2}{(\omega^2 + \frac{\rho_o\lambda}{\Lambda})^2 + (\frac{\beta-\rho_o}{\Lambda}\,\omega)^2} \quad . \tag{B20}$$

If we neglect the effect of delayed neutrons we may assume $\omega >> \lambda$ and $\omega^2 >> \rho_o\lambda/\Lambda$ and we have

$$|H_s(\omega)|^2 = \frac{1}{\omega^2 + (\frac{\beta-\rho_o}{\Lambda})^2}$$

$$= \frac{1}{\omega^2 + \left[\frac{\beta}{\Lambda}\,(1-\frac{\rho_o}{\beta})\right]^2}$$

$$= \frac{1}{\omega^2 + (\frac{\beta}{\Lambda})^2(1-\$)^2}$$

$$= \frac{1}{\alpha_c^2}\,\frac{1}{(1-\$)^2 + (\omega/\alpha_c)^2} \quad , \tag{B21}$$

where

$\$ = \rho_o/\beta$ = subcriticality in dollars,

and

$\alpha_c = \frac{\beta}{\Lambda}$ = prompt neutron decay constant.

B. Reactivity Transfer Function

To derive the reactivity transfer function let

$$n = n_o + \delta n \tag{B22}$$

$$C = C_o + \delta C \tag{B23}$$

$$\rho = \rho_o + \delta\rho \quad . \tag{B24}$$

The point reactor kinetic equations in this case are

$$\frac{dn}{dt} = \frac{\rho k}{\ell} n - \frac{\beta k}{\ell} n + \lambda C + S \tag{B25}$$

$$\frac{dC}{dt} = \frac{k\beta}{\ell} n - \lambda C \ . \tag{B26}$$

Substituting Equations B22, B23 and B24 in Equations B25 and B26 we have

$$\frac{d}{dt}\delta n = \frac{k}{\ell}(\rho_o+\delta\rho)(n_o+\delta n) - \frac{\beta k}{\ell} n_o - \frac{\beta k}{\ell}\delta n + \lambda C_o + \lambda\delta C + S$$

$$\approx \frac{k}{\ell}\rho_o n_o + \frac{k}{\ell}\rho_o\delta n + \frac{k}{\ell} n_o\delta\rho - \frac{\beta k}{\ell} n_o - \frac{\beta k}{\ell}\delta n + \lambda C_o$$

$$+ \lambda\delta C + S \tag{B27}$$

$$\frac{d}{dt}\,\delta C = \frac{k\beta}{\ell}\,n_o + \frac{k\beta}{\ell}\,\delta n - \lambda C_o - \lambda\delta C \ . \qquad \text{(B28)}$$

At steady state Equations B27 and B28 reduce to

$$0 = \frac{k}{\ell}\,\rho_o n_o - \frac{\beta k}{\ell}\,n_o + \lambda C_o + S \qquad \text{(B29)}$$

$$0 = \frac{k\beta}{\ell}\,n_o - \lambda C_o \ . \qquad \text{(B30)}$$

Solving for S we have

$$S = -\frac{k}{\ell}\,\rho_o n_o \ . \qquad \text{(B31)}$$

Substituting in Equations B27 and B28 and introducing new variable $\Lambda = \ell/k$, we have

$$\frac{d}{dt}\,\delta n = \frac{\rho_o}{\Lambda}\,\delta n + \frac{n_o}{\Lambda}\,\delta\rho - \frac{\beta}{\Lambda}\,\delta n + \lambda\delta C \qquad \text{(B32)}$$

$$\frac{d}{dt}\,\delta C = \frac{\beta}{\Lambda}\,\delta n - \lambda\delta C \ . \qquad \text{(B33)}$$

Taking Laplace transforms of Equations B32 and B33, we have

$$s\Delta N(s) = \frac{\rho_o}{\Lambda}\,\Delta N(s) + \frac{n_o}{\Lambda}\,\Delta\rho(s) - \frac{\beta}{\Lambda}\,\Delta N(s) + \lambda\Delta C(s) \qquad \text{(B34)}$$

$$s\Delta C(s) = \frac{\beta}{\Lambda}\,\Delta N(s) - \lambda\Delta C(s) \ . \qquad \text{(B35)}$$

Solving for $\Delta C(s)$ in Equation B35 and then substituting in Equation B34 and rearranging we finally find the transfer function as

$$H_r(s) = \frac{\Delta N(s)}{\Delta R(s)} = \frac{n_o}{\Lambda} \frac{1}{s - \frac{\rho_o}{\Lambda} + \frac{\beta}{\Lambda} - \frac{\lambda\beta}{\Lambda(s+\lambda)}} \quad . \tag{B36}$$

Multiplying the numerator and denominator of Equation B36 by $(s+\lambda)$ and assuming that $\lambda << \frac{\rho_o - \beta}{\Lambda}$, we have

$$H_r(s) = \frac{n_o}{\Lambda} \frac{s + \lambda}{s^2 + (\frac{\beta - \rho_o}{\Lambda})s - \frac{\rho_o \lambda}{\Lambda}} \quad . \tag{B37}$$

Assuming that $\omega >> \lambda$ and taking the square modulus of Equation B37, we finally have

$$|H_r(\omega)|^2 = (\frac{n_o}{\beta})^2 \frac{1}{(1-\$)^2 + (\frac{\omega}{\alpha_c})^2} \quad . \tag{B38}$$

For a critical reactor $\$=0$ and Equation B38 reduces to

$$|H_r(\omega)|^2 = (\frac{n_o}{\beta})^2 \frac{1}{1 + (\frac{\omega}{\alpha_c})^2} \quad . \tag{B39}$$

XIV. APPENDIX C: CROSS SPECTRAL DENSITY FORMULATION

Figure C1 shows two non-identical detection signal processing systems which have as inputs the sum of a common signal, $i(t)$, and an uncorrelated signal, $Z_n(t)$, for each channel, where $n = x,y$ refers to channels x and y. Note that $i(t)$, $Z_x(t)$ and $Z_y(t)$ have no correlation with each other. When the convolution integral is applied, it is found that

$$x(t) = \int_{-\infty}^{\infty} h_{dx}(u)\,[Z_x(t-u) + W_x\, i(t-u)]\,du\ , \qquad \text{(C1)}$$

and

$$y(t) = \int_{-\infty}^{\infty} h_{dy}(v)\,[Z_y(t-v) + W_y\, i(t-v)]\,dv, \qquad \text{(C2)}$$

where W_x and W_y are detection efficiencies.

The cross-correlation function of $x(t)$ and $y(t)$ is by definition

$$\phi_{xy}(\tau) = \lim_{T\to\infty} \frac{1}{2T} \int_{-T}^{T} x(t)y(t+\tau)\,dt$$

$$= \lim_{T\to\infty} \frac{1}{2T} \int_{-T}^{T}\int_{-\infty}^{\infty}\int_{-\infty}^{\infty} h_{dx}(u)h_{dy}(v)\,[Z_x(t-u)+W_x i(t-u)]$$

$$[Z_y(t+\tau-v) + W_y\, i(t+\tau-v)\,dudvdt$$

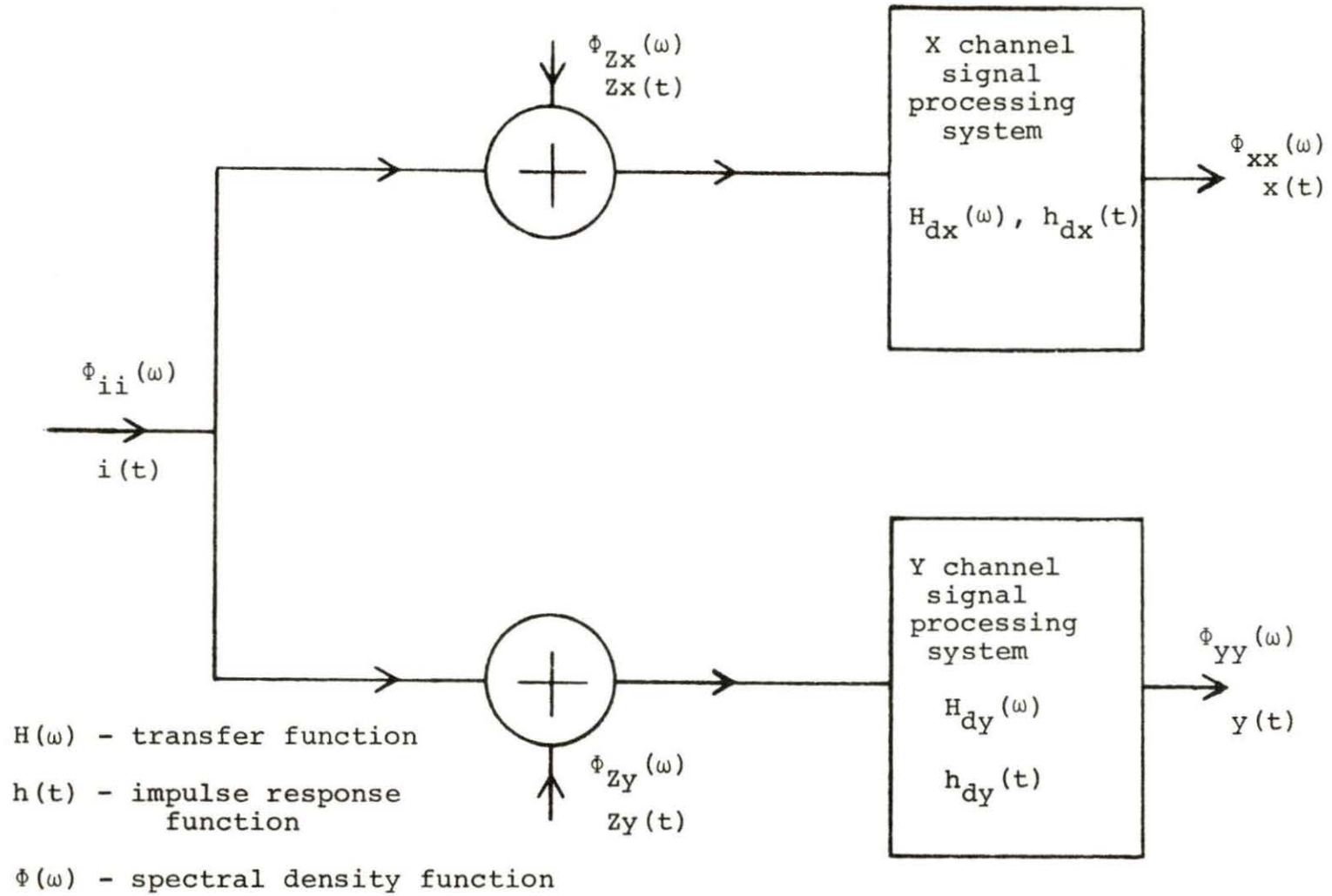

Figure C1. Signal processing system

$$= \lim_{T\to\infty} \frac{1}{2T} \int_{-T}^{T}\int_{-\infty}^{\infty}\int_{-\infty}^{\infty} h_{dx}(u)h_{dy}(v)[Z_x(t-u)Z_y(t+\tau-v) +$$

$$W_y Z_x(t-u)i(t+\tau-v) + W_x i(t-u)Z_y(t+\tau-v) +$$

$$W_x W_y i(t-u)i(t+\tau-v)]dudvdt$$

$$= \int_{-\infty}^{\infty}\int_{-\infty}^{\infty} h_{dx}(u)h_{dy}(v) \left[\lim_{T\to\infty} \frac{1}{2T} \int_{-T}^{T} [Z_x(t-u)Z_y(t+\tau-v) +\right.$$

$$W_y Z_x(t-u)i(t+\tau-v) + W_x i(t-u)Z_y(t+\tau-v) +$$

$$\left. W_x W_y\, i(t-u)i(t+\tau-v)]dt\right] dudv$$

$$= \int_{-\infty}^{\infty}\int_{-\infty}^{\infty} h_{dx}(u)h_{dy}(v)\ [\phi_{Z_x Z_y}(\tau+u-v) +$$

$$W_y \phi_{Z_x i}(\tau+u-v) + W_x \phi_{i Z_y}(\tau+u-v) +$$

$$W_x W_y \phi_{ii}(\tau+u-v)]dudv. \qquad \text{(C3)}$$

Since $i(t)$, $Z_x(t)$, and $Z_y(t)$ are uncorrelated, $\phi_{Z_x Z_y}$, $\phi_{Z_x i}$ and $\phi_{i Z_y}$ are equal to zero, leaving the cross-correlation of $x(t)$ and $y(t)$ as

$$\phi_{xy}(\tau) = \int_{-\infty}^{\infty}\int_{-\infty}^{\infty} h_{dx}(u)h_{dy}(v)\ W_x W_y \phi_{ii}(\tau+u-v) \qquad \text{(C4)}$$

The cross-spectral density function is the Fourier transform of the cross-correlation function, or

$$\Phi_{xy}(\omega) = \int_{-\infty}^{\infty} \phi_{xy}(\tau)\, e^{-j\omega\tau}\, d\tau$$

$$= W_x W_y \int_{-\infty}^{\infty}\int_{-\infty}^{\infty}\int_{-\infty}^{\infty} h_{dx}(u) h_{dy}(v) \phi_{ii}(\tau+u-v) e^{-j\omega\tau}\, dudvd\tau. \quad (C5)$$

If a change in variables is made, $\Delta = \tau+u-v$, then $\tau = \Delta+v-u$, and

$$\Phi_{xy}(\omega) = W_x W_y \int_{-\infty}^{\infty}\int_{-\infty}^{\infty}\int_{-\infty}^{\infty} h_{dx}(u) h_{dy}(v) \phi_{ii}(\Delta) e^{-j\omega(\Delta+v-u)} dudvd\Delta$$

$$= W_x W_y \int_{-\infty}^{\infty} h_{dx}(u) e^{j\omega u}\, du \int_{-\infty}^{\infty} h_{dy}(v) e^{-j\omega v}\, dv.$$

$$\int_{-\infty}^{\infty} \phi_{ii}(\Delta) e^{-j\omega\Delta}\, d\Delta$$

$$= W_x W_y H_{dx}^{*}(\omega) H_{dy}(\omega) \Phi_{ii}(\omega) . \quad (C6)$$

where * signifies the complex conjugate.

Assuming that the signal processing systems only affect the gain of the signals we have

$$H_{dx}^{*}(\omega) = A_x(\omega) H_d^{*}(\omega) , \quad (C7)$$

and

$$H_{dy}(\omega) = A_y(\omega) H_d(\omega). \quad (C8)$$

And finally the cross spectral density of the two signals x(t) and y(t) could be written as

$$\Phi_{xy}(\omega) = W_x W_y A_x(\omega) A_y(\omega) |H_d(\omega)|^2 \Phi_{ii}(\omega). \qquad \text{(C9)}$$

XV. APPENDIX D: SUBCRITICAL REACTIVITY FORMULATIONS

For the case of identical detectors the plateau values of the coherence function for the cases of subcritical and critical reactor can be found from Equations 47 and 48 as

$$\gamma_{s,o} = \frac{Q_{m,c}}{(1-\$)^2 + Q_{m,c}} , \tag{D1}$$

and

$$\gamma_{c,o} = \frac{Q_{m,c}}{1 + Q_{m,c}} . \tag{D2}$$

$Q_{m,c}$ can be eliminated in the above two equations giving \$ in terms of $\gamma_{s,o}$ and $\gamma_{c,o}$:

$$\$(\gamma_{c,o},\gamma_{s,o}) = 1 - \left[\frac{\gamma_{c,o}}{1-\gamma_{c,o}} \frac{1-\gamma_{s,o}}{\gamma_{s,o}}\right]^{1/2} \tag{D3}$$

For the case of non-identical detectors the plateau values of the coherence functions for the cases of subcritical and critical reactor can be found from Equations 52 and 53 as

$$\gamma_{s,o} = \frac{Q_{x,m,c} \cdot Q_{y,m,c}}{[(1-\$)^2 + Q_{x,m,c}][(1-\$)^2 + Q_{y,m,c}]}^{1/2} , \tag{D4}$$

and

$$\gamma_{c,o} = \left[\frac{Q_{x,m,c} \cdot Q_{y,m,c}}{(1 + Q_{x,m,c})(1 + Q_{y,m,c})}\right]^{1/2} . \tag{D5}$$

After squaring Equation D5 and dividing the numerator and denominator of the right hand side by $Q^2_{y,m,c}$ we have

$$\gamma^2_{c,o} = \frac{r}{(r + 1/Q_{y,m,c})(1 + 1/Q_{y,m,c})} . \quad (D6)$$

Equation D6 can be solved for $Q_{y,m,c}$ giving

$$Q_{y,m,c} = \gamma_{c,o} \frac{(1+r)\gamma_{c,o} + [(1-r)^2\gamma^2_{c,o} + 4r]^{1/2}}{2r(1 - \gamma^2_{c,o})} . \quad (D7)$$

After squaring Equation D4 and dividing the numerator and denominator of the right hand side by $Q^2_{y,m,c}$ we have

$$\gamma^2_{s,o} = \frac{r}{\left[r + \frac{(1-\$)^2}{Q_{y,m,c}}\right]\left[1 + \frac{(1-\$)^2}{Q_{y,m,c}}\right]} . \quad (D8)$$

Equation D8 can be solved for \$ giving

$$\$ = 1 - \left\{\frac{Q_{y,m,c}}{2\gamma_{s,o}} \left[[\gamma^2_{s,o}(1-r)^2 + 4r]^{1/2} - \gamma_{s,o}(1+r)\right]\right\}^{1/2} . \quad (D9)$$

$Q_{y,m,c}$ can be substituted in from Equation D7 to yield the subcriticality as

$$\$(\gamma_{c,o},\gamma_{s,o},r) = 1 - \left[\gamma_{c,o}\,\frac{(1+r)\gamma_{c,o} + [(1-r)^2\gamma_{c,o}^2 + 4r]^{1/2}}{2r[1-\gamma_{c,o}^2]}\right.$$

$$\left.\times\,\frac{[(1-r)^2\gamma_{s,o}^2 + 4r]^{1/2} - (1+r)\gamma_{s,o}}{2\gamma_{s,o}}\right]^{1/2} . \qquad \text{(D10)}$$

For the case of $W_x = W_y = W$, but $W_s \neq W_c$, an equation for the subcriticality can be found in the following manner. Equation 46 can be rewritten in the following fashion

$$Q_{m,c} = \frac{DW_c}{R\beta^2} , \qquad \text{(D11)}$$

and

$$Q_{m,s} = \frac{DW_s}{R\beta^2} . \qquad \text{(D12)}$$

$Q_{m,c}$ can be found from Equation D2 as

$$Q_{m,c} = \frac{\gamma_{c,o}}{1-\gamma_{c,o}} . \qquad \text{(D13)}$$

From Equations D11 and D13 it can be found that

$$\frac{D}{R\beta^2} = \frac{1}{W_c}\,\frac{\gamma_{c,o}}{1-\gamma_{c,o}} . \qquad \text{(D14)}$$

From Equation D1 it can be seen that

$$(1-\$)^2 = Q_{m,s}\left(\frac{1}{\gamma_{s,o}} - 1\right) . \qquad \text{(D15)}$$

Application of Equations D12 and D14 in Equation D15 gives the subcriticality as

$$\$ = 1 - \left(\frac{W_s}{W_c}\,\frac{\gamma_{c,o}}{1-\gamma_{c,o}}\,\frac{1-\gamma_{s,o}}{\gamma_{s,o}}\right)^{1/2} . \qquad \text{(D16)}$$

Finally for the general case of $W_x \neq W_y$ and $W_{n,s} \neq W_{n,c}$ the subcriticality can be found in the following fashion. From Equations D8 and D9 we can deduce that

$$\$ = 1 - \left(\frac{Q_{y,m,s}}{2\gamma_{s,o}}\left[\left[\gamma_{s,o}^2(1-r_s)^2 + 4r_s\right]^{1/2} - \gamma_{s,o}(1+r_s)\right]\right)^{1/2}, \qquad \text{(D17)}$$

where

$$Q_{y,m,s} = \frac{DW_{y,s}}{R\beta^2} , \qquad \text{(D18)}$$

and

$$r_s = \frac{W_{x,s}}{W_{y,s}} . \qquad \text{(D19)}$$

From Equations D6 and D7 it can be found that

$$Q_{y,m,c} = \gamma_{c,o}\,\frac{(1+r_c)\gamma_{c,o} + \left[(1-r_c)^2\gamma_{c,o}^2 + 4r_c\right]^{1/2}}{2r_c(1-\gamma_{c,o}^2)}, \qquad \text{(D20)}$$

where

$$Q_{y,m,c} = \frac{DW_{y,c}}{R\beta^2} , \qquad \text{(D21)}$$

and

$$r_c = \frac{W_{x,c}}{W_{y,c}} \quad . \tag{D22}$$

From Equation D21 it can be seen that

$$\frac{D}{R\beta^2} = \frac{Q_{y,m,c}}{W_{y,c}} \quad . \tag{D23}$$

Application of Equation D23 in Equation D18 and use of Equation D20 gives

$$Q_{y,m,s} = \frac{W_{y,s}}{W_{y,c}} \gamma_{c,o} \frac{(1+r_c)\gamma_{c,o} + [(1-r_c)^2\gamma_{c,o}^2 + 4r_c]^{1/2}}{2r_c(1 - \gamma_{c,o}^2)} \tag{D24}$$

Insertion of Equation D24 in Equation D17 gives the desired equation for subcriticality.

XVI. APPENDIX E: THEORETICAL COHERENCE FUNCTION FORMULATION

The square modulus of the reactor transfer function defined by Equation 11 was found with the assumption that $\omega >> \lambda$, i.e. the effect of delayed neutrons were ignored. Yasuda and Miyoshi [36] suggest that in a graphite moderated reactor the mean lifetime of precursors to the short-lived delayed neutron emitters is not sufficiently longer than the lifetime of prompt neutrons. This complicates the separation of the prompt neutron decay mode from the associated delayed neutron mode.

In this section a "theoretical" coherence function is formulated using the transfer function given by Equation 12 which includes the effect of six delayed neutron groups. But the noise equivalent source spectral density which is used is that of Equation 6 which does not include the effect of delayed neutrons.

The coherence function was defined by Equation 41 as

$$\gamma(\omega) = \left(\frac{Q_x(\omega) \cdot Q_y(\omega)}{[1 + Q_x(\omega)][1 + Q_y(\omega)]} \right)^{1/2} . \qquad (E1)$$

Using Equations 6, 17 and 30 and introducing the Bennett factor R we have

$$Q_n(\omega) = \frac{W_n |H_r(\omega)|^2_D}{Rn^2} \qquad (E2)$$

The reactor transfer function with six delayed neutron groups is given in expanded form by Schultz [28] as

$$H_r(s) = \frac{n}{\ell s} \frac{(s+\lambda_1)(s+\lambda_2)(s+\lambda_3)(s+\lambda_4)(s+\lambda_5)(s+\lambda_6)}{s^6+a_5s^5+a_4s^4+a_3s^3+a_2s^2+a_1s+a_o}, \qquad \text{(E3)}$$

where λ_i are delayed neutron precursors' decay constants and a_i are lengthy equations in terms of λ_i, β_i, the delayed neutron fractions and ℓ, the prompt neutron lifetime.

The square modulus of Equation E3 can be written in the form

$$|H_r(\omega)|^2 = \frac{n^2}{\ell^2} A(\omega) \ , \qquad \text{(E4)}$$

where $A(\omega)$ is the frequency dependent part of the square modulus of the transfer function.

Substituting Equation E2 and E4 in Equation E1 we have

$$\gamma(\omega) = DA(\omega) \left\{ \frac{W_x W_y}{[\ell^2 R + W_x DA(\omega)][\ell^2 R + W_y DA(\omega)]} \right\}^{1/2} . \qquad \text{(E5)}$$

The Diven factor D has a value of $\sim$0.8 for U^{235}, the Bennett factor has a value of $\sim$1.2. Since α_c, the prompt neutron decay constant can be found experimentally, ℓ can be estimated from equation $\ell = \beta/\alpha_c$, where β is the total delayed neutron fraction and will be assumed to be .0064. From Equation 33

$$Q_{n,m} = \frac{D}{R\beta^2} W_n,$$

the values W_x and W_y can be estimated since $Q_{n,man}$ can be found experimentally. Insertion of these values in Equation E5 gives a "theoretical" coherence function which estimates the effect of delayed neutrons.

XVII. APPENDIX F: RESULTS OF COHERENCE FUNCTION MEASUREMENT AT 4.5" FROM THE SOUTH TANK

The results of the coherence function measurement at 4.5" from the south core are given in Table F1, with the results of weighted least squares fitting of the experimental data and standard deviation of experimental data.

Table F1. Results of the coherence function measurement at 4.5" from the south core

Frequency Hz	Effective filter width, Hz	Gated scaler reading, C_S	Clock scaler reading, C_M	Experimental coherence function, $\bar{\gamma}$	Curve fitted coherence function, γ	Standard deviation $\sigma_{\bar{\gamma}}$
0.3	0.08	28196094	36042158	0.775	0.737	0.0546
0.4	0.08	27367357	36055861	0.726	0.737	0.0625
0.5	0.08	28195364	36051453	0.775	0.736	0.0546
0.6	0.08	28031529	36045940	0.765	0.736	0.0561
0.7	0.08	28396055	36039829	0.786	0.736	0.0527
0.8	0.08	28683535	36069371	0.800	0.735	0.0503
0.9	0.08	27758197	36052433	0.750	0.735	0.0587
1.0	0.08	27667836	36052034	0.744	0.734	0.0599
1.25	0.24	27332504	36053455	0.725	0.732	0.0362
1.5	0.24	27506109	36038315	0.737	0.730	0.0351
2.0	0.40	26921946	36057266	0.700	0.724	0.0298
2.5	0.40	27193060	36044126	0.718	0.717	0.0286
3.0	0.40	26879927	36063703	0.697	0.709	0.0299
4.0	0.80	26867416	36079905	0.695	0.688	0.0213
5.0	0.80	26433012	36057376	0.669	0.663	0.0225
6.0	0.80	25726437	36051710	0.622	0.635	0.0245
7.0	0.80	25114566	36069601	0.578	0.605	0.0263
8.0	0.80	24952071	36058804	0.567	0.573	0.0268
9.0	0.80	24587424	36060407	0.540	0.541	0.0278
10.0	0.80	24140546	36063116	0.508	0.510	0.0290
12.0	1.60	23435707	36075389	0.453	0.449	0.0218
14.0	1.60	22419697	36055453	0.3735	0.393	0.0236

16.0	1.60	22131434	36241315	0.342	0.344	0.0243
18.0	1.60	21486796	36063425	0.296	0.301	0.0251
20.0	1.60	21046639	36075955	0.259	0.265	0.0258
22.5	2.0	20718899	36072804	0.232	0.226	0.0235
25.0	2.0	20331992	36022623	0.201	0.195	0.0239
27.5	2.0	20123514	36008379	0.184	0.168	0.0242
30.0	4.0	19441914	36016603	0.124	0.147	0.0249
35.0	4.0	19354218	36079495	0.114	0.114	0.0177
40.0	4.0	19214403	36068451	0.103	0.0906	0.0178
50.0	8.0	19036514	36076719	0.0869	0.0606	0.0127
60.0	8.0	20089087	36074656	0.177	--	--
70.0	8.0	18513699	36088563	0.0408	0.0322	0.0129
80.0	8.0	18433221	36035257	0.0362	0.0249	0.0129
90.0	8.0	18274779	36003742	0.0216	0.0198	0.0130
100.0	8.0	18315013	36011376	0.0266	0.0162	0.0130